Title: A high-resolution analysis of arrestin2 interactions responsible for CCR5 endocytosis

Authors: Ivana Petrovic[1,*], Samit Desai[1], Polina Isaikina[1,†], Layara Akemi Abiko[1], Anne Spang[1,*] and Stephan Grzesiek[1,*]

Affiliations:
[1] Biozentrum, University of Basel, CH-4056 Basel, Switzerland

† present address: Center for Life Sciences, Paul Scherrer Institut, CH-5232 Villigen, Switzerland

*Corresponding authors. Email: stephan.grzesiek@unibas.ch, anne.spang@unibas.ch, ivana.petrovic@unibas.ch

Keywords: arrestin, G protein-coupled receptor (GPCR); CCR5; chemokines, clathrin-mediated endocytosis (CME), clathrin, Adaptor protein 2 (AP2) complex, NMR, microscopy

Abstract

Clathrin-mediated endocytosis (CME) is crucial for regulating G protein-coupled receptors (GPCRs) via phosphorylation-dependent arrestin interactions. The interplay between receptor phosphorylation and arrestin coupling to the CME machinery has only been explored for a few GPCRs. Here we have investigated the CME of the chemokine receptor CCR5 induced by native and engineered CCL5 ligands. Upon CCL5 agonist stimulation, arrestin2 translocates to CCR5 at the plasma membrane forming a long-lived CCR5-arrestin2 complex that is internalized but does not reach the lysosomes. Solution NMR revealed that arrestin2 interacts weakly with clathrin through a single binding site, independent of arrestin2 activation by phosphorylated CCR5 C-terminal tail peptides. In contrast, the arrestin2-AP2 interaction is stronger and requires arrestin2 activation depending quantitatively on the CCR5 C-terminal tail phosphorylation. The *in vitro* results are corroborated by cellular assays, which establish a crucial role of the arrestin2 interaction with AP2, but not with clathrin for CCR5 internalization. These findings give insights how receptor phosphorylation regulates arrestin-mediated GPCR internalization.

33 **Introduction**

34 G protein-coupled receptors (GPCRs) represent a large family of transmembrane cell surface
35 receptors that mediate the cellular response to a wide variety of signals, including hormones,
36 neurotransmitters, and sensory stimuli. Their crucial role in many human physiological
37 processes makes them an important drug target with more than 30% of existing small-molecule
38 drugs binding to GPCRs.[1] To ensure precise signal transduction the receptor signaling cascade
39 events must be tightly regulated. This is achieved by coordinating receptor interactions with
40 various intracellular proteins, including G proteins,[2] GPCR kinases (GRKs),[3] and arrestins,[4]
41 with the latter eventually leading to receptor internalization in a process known as endocytosis.
42 Endocytosis is a major mechanism of GPCR signal downregulation.[5] However, some receptors
43 rapidly recycle back to the plasma membrane,[5] which may also serve to scavenge external
44 ligands and degrade them within the lysosomes.[6,7]

45 Although GPCR endocytosis can occur through several different pathways, the vast majority
46 of GPCRs are internalized by clathrin-mediated endocytosis (CME).[8] This process relies on the
47 clathrin protein for the formation of vesicular structures from the plasma membrane that later
48 mature into endosomes.[9,10] While clathrin exhibits a diverse interaction spectrum,[11,12] it cannot
49 directly interact with the membrane receptors or plasma membrane lipids and requires adaptor
50 proteins to select its internalization cargo.[8,13–15]

51 The adaptor complex 2 (AP2) plays a central role in the formation of the clathrin-coated
52 vesicles[16] and the selection of the cargo molecules.[17] It consists of two large (α and β2) and two
53 smaller (μ2 and σ2) subunits.[18] While each subunit plays a role in CME,[19] recognition of
54 endocytic cargo motifs has been attributed to the σ2 subunit (LL-motif) and μ2 subunit (YxxΦ-
55 motif).[20]

56 For some GPCRs, such as the protease-activated receptor 1 (PAR1), the direct interaction
57 with AP2 is sufficient for receptor internalization.[21,22] However, the majority of GPCRs require
58 arrestins as endocytic adaptors for internalization.[23] The non-visual arrestins, arrestin2 and

59 arrestin3, bind to non-visual GPCRs upon intracellular phosphorylation,[4] participate in signaling
60 events,[24] and can mediate receptor internalization through direct interaction with clathrin[25,26]
61 and the β2 subunit of the AP2 complex.[27]

62 Once internalized, receptors are either recycled back to the plasma membrane or sent for
63 lysosomal degradation with the notion that the stability of the arrestin complex potentiates
64 intracellular receptor sequestration.[28] According to the strength and persistence of arrestin
65 interactions, GPCRs have been categorized into class A and class B subtypes.[28,29] To distinguish
66 these classes from the common IUPHAR classification of GPCRs, we refer in the following to
67 the arrestin classes as arr-class A and B, respectively. Arr-class A receptors (e.g. adrenergic
68 receptors) form transient complexes with arrestins that quickly dissociate near the plasma
69 membrane and the receptor traffics alone into endosomes. In contrast, arr-class B receptors (e.g.
70 the vasopressin receptor 2, V2R) have a higher affinity towards arrestin and form long-lived
71 complexes that traffic together into endosomes.[28]

72 The human chemokine receptor 5 (CCR5) is a GPCR, which acts as the main HIV co-
73 receptor[30] and plays a central role in inflammation,[31] COVID-19 infection,[32] chronic diseases,[31]
74 as well as cancer.[33] We have recently investigated the phosphorylation and arrestin2 interactions
75 of CCR5.[29] This revealed a key pXpp GPCR phosphorylation motif in its C-terminal tail, which
76 is specifically recognized by well-defined interactions of individual phosphates with positively
77 charged arrestin2 residues. The pXpp motif is also observed in many other receptors[34] known
78 to form a stable complex with arrestin2.[35–37] Moreover, the strength of the arrestin interaction
79 could be correlated to the phosphosite density and its distribution on the receptor C-terminal tail
80 and intracellular loops,[29,38] thus assigning the receptors with high phosphosite density (including
81 CCR5) to the arr-class B subtype. While our findings demonstrated how multi-site
82 phosphorylation controls GPCR-arrestin interactions, the interplay between arrestin activation
83 by receptor phosphorylation and its interactions with the clathrin/AP2 complex responsible for
84 internalization remains poorly understood.

85 Here we have characterized the chemokine-induced internalization of CCR5 in cellular
86 assays and the interactions of arrestin2 with clathrin and AP2 as a function of arrestin2 activation
87 by the phosphorylated CCR5 C-terminal tail. The results give insights how variation in receptor
88 phosphorylation propensities leads to the observed differences in arrestin-mediated arr-class A
89 and B GPCR internalization.

90 **Results**

91 **Ligand-dependent CCR5 internalization monitored in HeLa cells**

92 Previous reports indicated that CCR5 undergoes CME[39] and that interactions with arrestin2
93 and arrestin3 are essential for this process.[40] We recently established that the phosphorylated
94 CCR5 C-terminus forms a high-affinity complex with arrestin2.[29] To better understand the
95 downstream interaction with the endocytic machinery, we monitored CCR5 internalization upon
96 chemokine stimulation in HeLa (CCL2, ATCC nomenclature) cells (Fig. 1). HeLa cells were
97 transiently transfected with plasmids containing C-terminally FLAG-tagged CCR5 and YFP-
98 tagged arrestin2 (arrestin2-YFP) genes. This receptor construct was used to minimize CCR5
99 modifications and monitor the arrestin2 interaction in conditions as close to native as possible.
100 Before the addition of the chemokine ligands (0 min), CCR5 was observed at the plasma
101 membrane (magenta), while arrestin2 (green) was distributed throughout the cell (Fig. 1a-c).
102 Cells stimulated with the antagonist chemokine [5P12]CCL5[41] retained this CCR5 and arrestin2
103 distribution even 30 min after ligand addition (Fig. 1a). In contrast, when cells were stimulated
104 with the native agonist chemokine CCL5[42] (Fig. 1b) or the super-agonist [6P4]CCL5[41,43] (Fig.
105 1c), recruitment of arrestin2 from the cytoplasm to the plasma membrane could be detected
106 within 10 min. Prolonged ligand incubation times (30 min) lead to CCR5 internalization in
107 complex with arrestin2. To eliminate the possibility that arrestin2 recruitment to the membrane
108 was due to interactions with endogenous proteins in HeLa cells, we monitored internalization in
109 cells transfected only with arrestin2. In this case, the cells did not show characteristic arrestin2
110 recruitment to the plasma membrane or robust puncta formation, indicative of endosomes, even

111 in the presence of the super-agonist (Supplementary Fig. 1a). This control experiment also
112 revealed a few internal arrestin puncta devoid of receptor, presumably due to the arrestin2
113 overexpression. This phenomenon was also observed previously.[28,44]

114 Stronger phosphorylation and arrestin2/3 recruitment potencies have been reported for
115 [6P4]CCL5 as compared to wild-type CCL5.[45] In agreement with this, [6P4]CCL5 appears more
116 potent than CCL5 in recruiting arrestin2 to the plasma membrane and inducing CCR5-arrestin2
117 puncta formation after 10 min (Fig 1b,c). However, 30 min after stimulation, no significant
118 difference in CCR5 and arrestin2 colocalization was observed as quantified by the Mander's
119 coefficient (Fig. 1d). The Manders's coefficient is about 0.7 in cells stimulated by either agonist,
120 but close to zero for non-stimulated or antagonist-incubated cells (Fig. 1d). Apparently the two
121 agonist ligands induce a differing initial rate of arrestin2 recruitment by CCR5. However, once
122 arrestin2 is recruited, the CCR5-arrestin2 complex accumulates and remains stable for at least
123 30 min inside the cells.

124 To further corroborate the arr-class B-like behavior of CCR5, we counted the puncta positive
125 for CCR5 or both CCR5 and arrestin2 in cells at this time point after stimulation by [6P4]CCL5
126 (Fig. 1e). No significant difference was observed between the two values. This indicates that the
127 number of puncta containing only CCR5, but not arrestin2, must be very small and that the
128 majority of CCR5 puncta also contains arrestin2, consistent with stable complex formation.
129 Furthermore, the CCR5 and arrestin2 colocalization occurs not only close to the plasma
130 membrane but also close to the nucleus (Fig. 1f), indicative of the arr-class B-like behavior of
131 CCR5. For arr-class A receptors, it would be expected that arrestin2 is excluded from receptor-
132 containing structures, which traffic into the perinuclear region.[28]

133 As both recycling[7,46] and degradation[7] has been observed during CCR5 internalization, the
134 cellular fate of the CCR5-arrestin2 complex was probed using the lysosomal-associated
135 membrane protein 1 (LAMP1) as a marker of the lysosomal membranes (Fig. 1g). No
136 recruitment of the complex to the lysosomes (LAMP1, yellow) was detected in the presence of

137 [6P4]CCL5 even 30 min after ligand stimulation. Similar results were obtained for both CCL5
138 and [6P4]CCL5 using the LysoTracker™ dye that accumulates in acidic environments, such as
139 the lysosome (Supplementary Fig. 1b,c). These results indicate that the CCR5 internalization
140 pathway, although mediated by arrestin, does not lead to rapid receptor degradation in
141 lysosomes.

142 **Localizing and quantifying the arrestin2-clathrin interaction by NMR spectroscopy**

143 As CCR5 relies on arrestin2 for internalization[40] and utilizes clathrin-mediated pathways,[39]
144 we investigated the consequences of the CCR5-arrestin2 coupling on the interaction with
145 clathrin and AP2 proteins. Arrestin2 consists of two consecutive (N- and C-terminal) β-
146 sandwich domains (Fig. 2a), followed by the disordered clathrin-binding loop (CBL, residues
147 353–386), strand β20, and a disordered C-terminal tail after residue 393. The CBL contains a
148 clathrin-binding motif ([L/I]ΦXΦ[D/E] where X denotes any amino acid and Φ is a bulky
149 hydrophobic residue[11,19] (Supplementary Fig. 2a). Strand β20 forms a characteristic β-sheet with
150 the N-terminal strand β1 in inactive arrestin. Upon activation, the phosphorylated receptor tail
151 replaces β20 in the β-sheet and releases it from the arrestin core.

152 A structure of a complex between arrestin2 and the clathrin heavy chain N-terminal domain,
153 (residues 1-363, CLTC NTD) has been solved by X-ray crystallography (PDB:3GD1).[47] The
154 structure (Supplementary Fig. 2b-d) suggests a 2:1 binding model between arrestin2 and the
155 CLTC NTD. The first interaction occurs between the clathrin-binding motif of the arrestin2
156 CBL and the edge of the first two β-sheet blades of the CLTC NTD. This CLTC region is also
157 known to interact with many other proteins.[11] The second interaction is found between the splice
158 loop of the arrestin2 C-terminal β-sandwich and the 4th and 5th blade of the CLTC NTD. The
159 3GD1 structure had been solved in the absence of an arrestin2-activating phosphopeptide.

160 To elucidate the clathrin-arrestin interactions under solution conditions and the influence of
161 arrestin activation we utilized NMR spectroscopy. Fig. 2b depicts part of a ^{1}H-^{15}N TROSY
162 spectrum (full spectrum in Supplementary Fig. 3a) of the truncated ^{15}N-labeled arrestin2

163 construct arrestin2$^{1-393}$ (residues 1-393), which comprises the C-terminal strand β20, but lacks
164 the disordered C-terminal tail. Due to intrinsic microsecond dynamics, the assignment of the
165 ^{1}H-^{15}N resonances by triple resonance methods was so far possible only for 16 residues (residues
166 367-381, 385-386) within the mobile CBL. Whereas this region of arrestin is typically not
167 visible in either crystal or cryo-EM structures due to its high flexibility, it provides excellent
168 probes for solution NMR studies. The addition of an equimolar amount of CLTC NTD to
169 arrestin2$^{1-393}$ induced significant line broadening between residues T374 and T381 with I377
170 being the most strongly affected residue (Fig. 2c, Supplementary Fig. 3b). This region almost
171 exactly matches and fully comprises the canonical arrestin2 clathrin-binding motif ^{376}LIELD^{380}.
172 Fig. 2a shows these interacting residues mapped on an arrestin2 AlphaFold2 model.[48]

173 As ^{1}H-^{13}C methyl resonances have more favorable relaxation properties than backbone
174 ^{1}H-^{15}N resonances,[49] we used Ile-δ1-^{13}CH$_3$-labeled arrestin2 to quantitatively monitor the
175 formation of the arrestin2-clathrin complex (arrestin2 assignments transferred from BMRB,
176 ID:51131[50]). HMQC spectra of the 15 Ile δ1-^{13}CH$_3$ methyl groups of arrestin2$^{1-393}$ (Fig. 2d)
177 revealed changes in peak intensity (Fig. 2e, top) and chemical shift perturbations (Fig. 2e,
178 bottom) only for I377 at an equimolar addition of unlabeled CLTC NTD to arrestin2$^{1-393}$. An
179 apparent dissociation constant $K_D = 104 \pm 9$ μM was determined from titrating CLTC NTD and
180 fitting the arrestin2 I377 ^{13}C chemical shifts with a 1:1 binding isotherm (Fig. 2f). Although the
181 formed complex (total molecular weight 85 kDa) has low affinity, such interactions are common
182 in endocytosis, which involves many multi-site interactions within a large network of proteins.[19]

183 **The arrestin2-clathrin interaction is independent of arrestin2 activation**

184 Due to significant line broadening of the arrestin2 resonances upon phosphopeptide addition,
185 the influence of arrestin activation on the clathrin interaction could not be detected on either
186 backbone or methyl resonances. However, the CLTC NTD, although similar in size to
187 arrestin2$^{1-393}$ (41 kDa vs. 44 kDa), provided considerably better ^{1}H-^{15}N TROSY spectra due to
188 the absence of significant micro- to millisecond dynamics. This allowed to observe the effect of

189 arrestin2 activation on its interaction with clathrin by titrating arrestin2$^{1-393}$ to ^{15}N-labeled CLTC
190 NTD. Fig. 3a (left) shows the intensity changes (full spectra in Supplementary Fig. 4a) of the
191 CLTC NTD ^{1}H-^{15}N TROSY resonances (assignments transferred from BMRB, ID:25403[51])
192 upon addition of a one-molar equivalent of arrestin2$^{1-393}$. A significant intensity reduction due
193 to line broadening is detected for CLTC residues 39-40, 48-50, 62-72, 83-90, 101-106, and 108.
194 These residues form a clearly defined binding region at the edges of blade 1 and blade 2 of the
195 CLTC NTD (Fig. 3a, right), which corresponds to the first interaction site observed in the 3GD1
196 crystal structure. However, no significant signal attenuation was observed for residues of the
197 second crystal interaction site between blade 4 and blade 5 (in proximity of residues 190 and
198 230), indicating that there is only one arrestin2 binding site in CLTC NTD. The second binding
199 site in the crystal structure may thus result from arrestin crystal packing.

200 Next, we tested whether the arrestin2-CLTC NTD interaction is enhanced in the presence of
201 the fully phosphorylated CCR5 phosphopeptide (CCR5pp6, where 6 indicates the number of
202 phosphosites, Supplementary Table 1), which displaces arrestin2 strand β20 by forming an
203 antiparallel β-sheet with strand β1, thereby activating arrestin2.[29] However, no additional signal
204 attenuation of the CLTC NTD ^{1}H-^{15}N resonances or extension to further CLTC NTD regions
205 was observed (Fig. 3b, Supplementary Fig. 4b), when arrestin2$^{1-393}$ was added in the presence
206 of a 5-molar equivalent of CCR5pp6 (corresponding to 80% of arrestin activation). Thus,
207 activation of arrestin2 has apparently no effect on the CLTC NTD interaction. These results
208 suggest that even for receptors with low phosphosite density, such as adrenergic and dopamine
209 receptors[29,38]), the arrestin2-clathrin interaction may still take place allowing efficient receptor
210 internalization.

211 Previous studies have suggested that the last residues of the arrestin2 C-terminus have an
212 inhibitory effect on clathrin binding.[52] We therefore tested the interaction of ^{15}N-labeled CLTC
213 NTD with full-length arrestin2 (arrestin2$^{1-418}$). However, the obtained residue intensity
214 attenuation was indistinguishable from the one observed for the arrestin2$^{1-393}$ construct (Fig. 3c,

215 Supplementary Fig. 4c). Therefore, the residues of the arrestin2 C-terminal tail do not interfere
216 with clathrin binding. In contrast, the interaction of clathrin with arrestin2 (Fig. 3d,
217 Supplementary Fig. 4d) was completely abolished when the arrestin2 clathrin-binding loop was
218 replaced by the loop of visual arrestin (arrestin2$^{\Delta CBL}$, construct details in Methods). The latter
219 loop lacks the clathrin-binding motif making visual arrestin incapable of interacting with
220 clathrin.[25]

221 Taken together, the solution NMR experiments reveal that arrestin2 interacts with the CLTC
222 NTD through a single binding site, independently of arrestin2 activation and the conformation
223 of the arrestin2 core.

224 **Arrestin activation is essential for AP2 interaction**

225 An equally important element of the endocytic pathway is the arrestin interaction with AP2.
226 The β2 subunit of the AP2 complex (AP2β2) interacts with the arrestin2/3 C-terminus,[27,53,54]
227 and a crystal structure of the complex between the AP2β2 C-terminal domain and a C-terminal
228 arrestin2 peptide (residues 383-402) comprising strand β20 has been solved (PDB: 2IV8).[17]
229 Interestingly, the C-terminal arrestin2 peptide forms a helical structure in the complex with AP2
230 (Fig. 4a) as opposed to its β-sheet coordination with strand β1 in inactive arrestin2. No
231 experimental data exist on the formation of the AP2-arrestin2 complex in the context of full-
232 length arrestin2 and its activation by phosphorylated receptor tails.

233 To test how different phosphorylation levels influence arrestin2 recruitment by the C-
234 terminal domain of AP2β2 (AP2β2$^{701-937}$, residues 701-937), we performed a SEC binding
235 assay. In the absence of phosphopeptide an equimolar mixture of 10 μM arrestin2$^{1-418}$ and 10
236 μM AP2β2 is separated into two peaks (Fig. 4b, orange), which elute at the positions
237 corresponding to the individual apo proteins (Fig. 4b, blue, green). Upon addition of 100 μM
238 CCR5pp6 (Fig. 4c, purple), an additional SEC peak appears at an elution volume of 2.6 ml,
239 which corresponds to the formed arrestin2-AP2β2 complex. Monotonously decreasing complex

240 yields were observed when reducing the amounts of CCR5pp6 added to the mixture (Fig. 4d),
241 and no complex formation occurred in the presence of 100 μM non-phosphorylated CCR5
242 phosphopeptide (CCR5pp0) (Fig. 4e). The dissociation constant of the CCR5pp6-arrestin2
243 complex was determined previously as 45 μM (Supplementary Table 1).[29] Not surprisingly, the
244 formation of the arrestin2-AP2β2 complex depends quantitatively on the affinity of the
245 phosphopeptide-arrestin2 complex. Correspondingly, the addition of the less phosphorylated
246 CCR5pp3 and CCR5pp4 with lower affinities towards arrestin2 (both K_D ~ 200 μM,
247 Supplementary Table 1),[29] resulted in a considerable, similar reduction of the formed arrestin2-
248 AP2β2 complex (Fig. 4f).

249 Using the extinction coefficients of all involved polypeptides, the apparent affinities
250 between AP2β2 and arrestin2 could be determined from the SEC profiles (Fig. 4g, see Methods
251 for details). In the presence of 100 μM CCR5pp6, this apparent K_D amounts to 9 μM. An
252 identical affinity value for the affinity between AP2β2 and an isolated arrestin β20 peptide
253 (residues 383-402, D402C) has been observed by EPR spectroscopy.[55] In the presence (100 μM)
254 of the less phosphorylated CCR5 peptides, the apparent AP2β2-arrestin2 affinities are reduced
255 by ~4–5 times (CCR5pp4: 44 μM, CCR5pp3: 40 μM), in good agreement with their ~4–5 times
256 reduced affinity for arrestin2.

257 It is interesting to note that CCR5pp3 and CCR5pp4 have similar affinities towards arrestin2
258 despite their different phosphorylation levels (3-fold vs. 4-fold phosphorylated), but only
259 CCR5pp3 contains the pXpp barcode which increases the arrestin2 activation, as assayed by the
260 binding of the Fab30 antibody.[29] Apparently, this barcode does not play a significant role in the
261 formation of arrestin2-AP2β2 complex as the complex formation appears solely governed by
262 the affinity of the phosphopeptide towards arrestin2.

263 To observe the atomic details of arrestin2 activation on its interaction with AP2β2, we used
264 ^{15}N-labeled AP2β2$^{701-937}$ (assignment transferred from BMRB ID:52320[56]). Upon addition of

265 arrestin2$^{1-418}$, no changes in the AP2β2 ^{1}H-^{15}N spectra are detected (Fig. 4h, Supplementary Fig.
266 5a), apparently due to the unavailability of arrestin2 β20 strand and C-terminal tail. However,
267 when arrestin2$^{1-418}$ was added in the presence of a 5-molar equivalent of CCR5pp6
268 (corresponding to 80% of arrestin activation), a significant intensity reduction due to line
269 broadening is detected for many AP2β2 ^{1}H-^{15}N resonances (Fig. 4i, left, Supplementary Fig.
270 5b). The strongest attenuated resonances clearly define a binding region within the C-terminal
271 domain of AP2β2 (Fig. 4i, right), which is an extension of the binding surface observed in the
272 crystal structure (PDB: 2IV8) of AP2β2 in complex with a 21-residue arrestin2 C-terminal
273 peptide comprising strand β20.[17] In agreement with the AP2β2 NMR observations, no
274 interaction was observed in the arrestin2 methyl and backbone NMR spectra upon addition of
275 AP2β2 in the absence of phosphopeptide (Supplementary Fig. 5c,d). However, the significant
276 line broadening of the arrestin2 resonances upon phosphopeptide addition (Supplementary Fig.
277 5e, f) precluded a meaningful assessment of the effect of the AP2β2 addition on arrestin2 in the
278 presence of phosphopeptide.

279 We then tested whether the presence of CLTC NTD influences complex formation between
280 arrestin2 and AP2β2, and vice versa. Arrestin2$^{1-418}$ does not form a complex in the SEC assay
281 with CLTC NTD (Supplementary Fig. 6a), which agrees with the weak affinity observed in the
282 NMR experiments (Fig. 2f). Furthermore, a SEC analysis of a mixture of arrestin2$^{1-418}$, CLTC
283 NTD, AP2β2$^{701-937}$, and CCR5pp6 (Supplementary Fig. 6b) indicates formation of a complex at
284 2.6 ml elution volume. An SDS analysis of this complex fraction showed the presence of
285 arrestin2$^{1-418}$ and AP2β2$^{701-937}$, but not of CLTC NTD (Supplementary Fig. 6c). This indicates
286 that CLTC NTD does not interact strongly with the arrestin2-AP2-CCR5 tail complex. As such
287 clathrin may not engage with the initial receptor internalization complex, but may be recruited
288 at later stages of the CME.

289 To test the stability of the formed arrestin2-AP2 interaction and its quaternary coordination,
290 we performed a trypsin proteolysis assay (Supplementary Fig. 7, uncropped gels in
291 Supplementary Fig. 8). Trypsin recognizes arrestin2 residue R393,[57] which is buried in the
292 arrestin2 apo state, but is involved in the interaction with AP2β2.[27] Without phosphopeptide,
293 the arrestin2$^{1-418}$ digestion midpoint occurs at 20-30 min due to the inaccessibility of the
294 cleavage site (Supplementary Fig. 7a-c). In the presence of a 5-molar equivalent of CCR5pp6
295 (Supplementary Fig. 7a), the top band corresponding to full-length arrestin2 has almost
296 completely disappeared (relative abundance 19%) already 5 min after incubation as a
297 consequence of the β20 strand release and the exposure of R393 to trypsin. However, the
298 presence of AP2β2$^{701-937}$ protects arrestin$^{1-418}$ from proteolysis, as evident from significantly
299 higher abundance at 5 min and a shift of the proteolysis midpoints to 10, 20, and 30 min at 1-,
300 2-, and 5-molar equivalents of AP2β2$^{701-937}$ respectively.

301 Analogous digestion experiments using CCR5pp3 (Supplementary Fig. 7b) or CCR5pp4
302 (Supplementary Fig. 7c) phosphopeptides revealed that they did not enhance the rate of arrestin2
303 proteolysis by trypsin at a 3-molar equivalent, as expected from their weaker affinity towards
304 arrestin2. In agreement with this, however, upon addition of 25-molar equivalents of either
305 peptide the rate of arrestin2 proteolysis was significantly increased, as full-length arrestin2
306 almost completely disappeared already 5 min after incubation. Thus as for CCR5pp6, the
307 presence of AP2β2$^{701-937}$ also protects arrestin$^{1-418}$ activated by CCR5pp3 or CCR5pp4 from
308 proteolysis.

309 In summary, these results indicate that arrestin2 activation by the binding of receptor
310 phosphopeptides and the subsequent release of its strand β20 is required for the interaction with
311 AP2. This interaction is modulated by the phosphorylation level of the receptor C-terminal
312 peptide and its relative abundance. The formed AP2 complex with arrestin is stable and more
313 resistant to proteolysis.

314 **Arrestin interaction with AP2 is essential for CCR5 internalization**

315 The interactions of arrestin with clathrin and AP2 have mostly been studied for the
316 internalization of the β2-adrenergic (β2AR)[23,44,47,54,58] and V2R[44,58] receptors. Here, we
317 investigated how both interactions affect the internalization of CCR5 in a HeLa KO cell line
318 (HeLa$^{-arr2/3}$) devoid of arrestin2 and arrestin3 as well as in HeLa (CCL2) cells (Fig. 5,
319 Supplementary Fig. 9, respectively).

320 To characterize the arrestin2-clathrin interaction, we generated a YFP-tagged arrestin2
321 construct with the clathrin-binding motif (arrestin2$^{\Delta LIELD}$-YFP) removed. No significant
322 difference in CCR5 internalization was detected in either HeLa cell line between wild-type
323 arrestin2-YFP and arrestin2$^{\Delta LIELD}$-YFP, when the cells were stimulated with [6P4]CCL5
324 (HeLa$^{-arr2/3}$: Fig. 5a-c, HeLa: Supplementary Fig. 9a). Apparently, the arrestin2-clathrin
325 interaction does not play a significant role in the internalization of the arr-class B CCR5
326 receptor. This is in contrast to findings for the arr-class A receptor β2AR where removal of the
327 LIELD motif impairs receptor internalization.[54]

328 To test the influence of the arrestin2-AP2 interaction, we introduced mutations within the
329 arrestin2 adaptin-binding motif, which is conserved across all arrestins (Supplementary Fig. 2a).
330 The mutation R395A within this motif has been found to inhibit β2AR internalization by
331 arrestin3.[27] Introducing the equivalent mutation into a fluorescent arrestin2 construct
332 (arrestin2^{R395A}-YFP), did not lead to significant changes in CCR5 internalization relative to
333 wild-type arrestin2-YFP (HeLa$^{-arr2/3}$: Fig. 5a-c, HeLa: Supplementary Fig. 9b).

334 The structure of AP2β2 in complex with the C-terminal arrestin2 peptide[17] shows arrestin2
335 residues D385, F388, F391, and R395 interacting via salt bridges and base stacking with AP2β2
336 (Fig. 4a). Apparently, these interactions lead to a rather stable complex of full-length arrestin2
337 with AP2β2$^{701-937}$ in solution as evidenced by our SEC binding assay, NMR and the protection
338 of activated arrestin2 against proteolysis (Fig. 4, Supplementary Fig. 7). We hypothesized that
339 due to this extended arrestin2-AP2β2 interaction interface, the mutation of a single interacting

340 residue may not suffice to inhibit the arrestin2-AP2 interaction leading to CCR5 internalization.
341 Hence, we generated a further arrestin2 mutant (arrestin2$^{\Delta AP2}$-YFP) with all four direct
342 interacting residues replaced (D385A, F388A, F391A, R395A). Similar to wild-type arrestin2-
343 YFP, arrestin2$^{\Delta AP2}$-YFP is recruited to CCR5 at the plasma membrane (HeLa: Supplementary
344 Fig. 9c). However, the subsequent CCR5 internalization is potently inhibited (HeLa$^{-arr2/3}$: Fig.
345 5a-c, HeLa: Supplementary Fig. 9d) as indicated by a reduction of the Mander's CCR5/arrestin2
346 colocalization coefficient (from ~0.8 to ~0.2) the number of puncta positive for CCR5 and
347 arrestin2 (from ~20–13 to ~8–6 per 100 μm^2, similar values obtained for CCR5 puncta). In
348 agreement with this finding, the arrestin2$^{\Delta AP2}$ mutant is unable to form a complex with AP2 in
349 the presence of CCR5pp6 as assayed by SEC (Supplementary Fig. 9e). Taken together, these
350 results show that the stable arrestin-AP2 interaction is crucial for CCR5 internalization, whereas
351 the arrestin-clathrin interaction is not critical for sequestration from the plasma membrane.

352 **Discussion**

353 In the present study, we have elucidated the role of CCR5 phosphorylation in arrestin-
354 clathrin and arrestin-AP2 interactions which are essential for CCR5 sequestration into cells.
355 Cellular experiments demonstrated chemokine agonist-induced recruitment of arrestin2 towards
356 CCR5 at the plasma membrane, which is followed by the sequestration of the CCR5-arrestin2
357 complex into the cytoplasm including the perinuclear region where it remains stable for an
358 extended period. This provides experimental evidence that CCR5 belongs to the arr-class B of
359 GPCRs as surmised previously from the large number of phosphorylation sites in its C-terminus
360 and the presence of the pXpp motif.[29] The sequestered receptor remained stable inside the cells
361 for at least 30 min, and was not rapidly degraded in lysosomes, even in the presence of
362 [6P4]CCL5. A similar CCR5 lysosome-evading internalization pattern has been observed for
363 the potent anti-HIV chemokine analog PSC-RANTES.[59] As a recent CCR5 trafficking study
364 demonstrated that CCR5 scavenges both CCL5 and [6P4]CCL5 chemokines in an arrestin-
365 dependent manner,[7] it is possible that the long retention of the CCR5-arrestin complex and the

366 ability of the receptor to undergo recycling[7,46] is utilized to remove the extracellular ligands
367 from the cell surface. This may help in the regulation of chemokine ligand concentrations.[60]
368 NMR and chromatographic data on arrestin2 interactions with clathrin and AP2 proteins in
369 the presence of arrestin2-activating CCR5 C-terminal phosphopeptides revealed the molecular
370 details underlying CCR5 sequestration. Whereas the analysis of arrestin2 ^{1}H-^{15}N resonances
371 was difficult due to significant line broadening from intrinsic microsecond dynamics,[29] the
372 better quality of the ^{1}H-^{15}N spectra of CLTC NTD allowed a detailed characterization of the
373 arrestin2-clathrin interaction from the clathrin side. Arrestin2 binds to clathrin with about 100
374 μM affinity. This interaction is independent of arrestin2 activation by phosphopeptides, which
375 may enable the internalization of receptors with low phosphorylation levels. The interaction is
376 mediated through a single binding site in a 1:1 stoichiometry involving the arrestin2 clathrin-
377 binding loop and the edges of blade 1 and blade 2 of the CLTC NTD. This binding site agrees
378 with one of the binding sites observed in the crystal structure of the arrestin2-CLTC NTD
379 complex (PDB: 3GD1),[47] but disagrees with the second crystal interaction site involving the
380 arrestin2 splice loop. Presumably, the latter is a result of crystal packing. Our findings are
381 supported by a recent study,[61] which suggests that the arrestin C-domain edge comprising the
382 splice loop anchors arrestin to the membrane. The membrane anchoring seems mutually
383 exclusive with clathrin binding.[61]
384 In contrast to the arrestin2-clathrin interaction, the arrestin2-AP2 interaction requires
385 arrestin2 activation by GPCR C-terminal tail phosphopeptides and depends quantitively on their
386 phosphorylation levels. The formed arrestin2-phosphopeptide-AP2 complexes are stable and
387 more resistant to proteolysis than binary arrestin2-phosphopeptide complexes. The dissociation
388 constant of the arrestin2-AP2 complex is about 10 μM in the presence of the fully
389 phosphorylated CCR5pp6, which is a 10-fold higher affinity than that of the arrestin2-clathrin
390 complex. This may indicate a preference towards AP2 complex formation for highly
391 phosphorylated receptors. However, as the phosphorylation decreases the arrestin2-AP2

392 dissociation constant weakens to about 40 μM, making it more comparable to the arrestin2-
393 clathrin interaction.

394 Based on the present CCR5 data, we envision the following CME mechanism, which may
395 also apply to other arr-class B receptors (Fig. 6, left). The high receptor phosphorylation leads
396 to a strong recruitment of arrestin even in the absence of interactions with negatively charged
397 PIP_2 in the plasma membrane.[62] The consequent tight binding of the phosphorylated receptor
398 tail to arrestin strand β1 stably activates arrestin thereby releasing its strand β20 and C-terminal
399 tail. The freed β20 strand can then interact with the β2 subunit of AP2, which becomes released
400 from the AP2 core upon AP2 activation by PIP_2 molecules.[16] Apparently, the interaction of
401 arrestin2 strand β20 with the AP2 β2 subunit is rather strong, since it could only be inhibited in
402 cellular assays by a fourfold, but not by a single mutation in the arrestin2 C-terminal region. In
403 contrast, removal of the clathrin-binding LIELD motif from arrestin2 did not impair receptor
404 internalization, which is in agreement with the determined relatively low affinity of the
405 arrestin2-clathrin interaction. This suggests that the clathrin interaction is less important for
406 receptor internalization than the AP2 interaction.

407 The AP2 activation by PIP_2 also exposes the AP2 clathrin-binding LLNLD motif,
408 responsible for clathrin recruitment and formation of the clathrin-coated pits.[16] In the stable
409 ternary complex of a highly phosphorylated arr-class B receptor with arrestin and AP2, the
410 exposed AP2 LLNLD clathrin-binding motif may then subsequently couple to the clathrin
411 network thereby inducing rapid sequestration from the plasma membrane into endosomes. The
412 direct clathrin interaction of arrestin via its LIELD motif appears less important in this respect.

413 Although the generalization of this mechanism from CCR5 to other arr-class B receptors has
414 to be explored further, it is indirectly corroborated in the visual rhodopsin-arrestin1 system. The
415 arr-class B receptor rhodopsin[29] also undergoes CME[55] with arrestin1 harboring the conserved
416 AP2 binding motif, but missing the clathrin-binding motif (Supplementary Fig. 2a). As arr-class
417 B receptors are almost all peptide-binding GPCRs,[28,29] we speculate that the strong arrestin

418 interaction may also be utilized to remove the extracellular ligands from the plasma membrane,
419 independent of receptor degradation.

420 In comparison to arr-class B receptors, arr-class A receptors have a lower phosphosite
421 density in their C-terminal tails. Previous studies on the arr-class A β2AR[27,47,54] revealed that
422 both clathrin and AP2 interaction are crucial for internalization. It is expected that the lower
423 phosphosite density of arr-class A receptors results in a less stable interaction with arrestin (Fig.
424 6, right). Therefore additional interactions with PIP_2 lipids are required to anchor arrestin to the
425 membrane and play a significant role in receptor endocytosis.[62] As a consequence of the low
426 phosphorylation of the receptor and the weakened interaction with arrestin strand β1, the
427 equilibrium between inactive (strand β20 forms β-sheet with β1) and active (β20 released)
428 arrestin is shifted towards the inactive conformation, even when arrestin is bound to the receptor
429 via core contacts. Due to the low availability of strand β20, the arrestin interaction with AP2 is
430 considerably weakened and comparable in strength to the clathrin interaction. This is consistent
431 with the finding that AP2 and clathrin participate with similar strength in arr-class A receptor
432 internalization.[27,47,54] However, as both interactions are weak, the sequestration is reduced. In
433 addition, the weaker receptor phosphorylation leads to fast dissociation of arrestin from the
434 receptor at or near the plasma membrane and in consequence the receptor traffics without
435 arrestin into endosomes.[28,38]

436 A recent study[63] using single-molecule microscopy and molecular dynamics simulations
437 suggests that arrestin3 preassociates with the plasma membrane and that, surprisingly, the
438 transient interaction with an active β_2-adrenergic receptor (arr-class A) activates arrestin3,
439 which then diffuses to CCPs (clathrin-coated pits) independently of the activating receptor. It is
440 conceivable, that also arrestin2 first gets activated by the phosphorylated CCR5 and then enters
441 the CCPs without receptor, having its β20 strand released and then interact with AP2 present in
442 the CCPs. However, our microscopic data rather indicate that CCR5 and arrestin2 colocalize
443 both at the membrane as well as in the cytosol at a later stage of the CME (Fig. 1b,c). It would

444 be interesting to obtain single-molecule microscopic data on the CCR5-arrestin2 system to allow
445 a stringent comparison with our high-resolution NMR data of the receptor tail, clathrin and AP2
446 interactions.

447 In conclusion, this biophysical and cellular analysis of the interactions between the CCR5,
448 arrestin2, and clathrin/AP2 endocytic machinery elucidates the interplay of forces driving GPCR
449 internalization. The strength of the receptor phosphorylation modulates the interaction with
450 arrestin2, the release of its strand β20, and subsequently its interaction with the β2 subunit of
451 AP2. In comparison, the arrestin2-clathrin interaction is weaker. The interaction between the
452 receptor phosphosites and arrestin appears as a distinctive factor between arr-class B and arr-
453 class A receptor sequestration, since phosphorylation of the latter is considerably weaker. These
454 findings expand on the previously suggested mechanism for the reduced sequestration of the
455 arr-class A receptor β2AR by the Kim & Benovic[54] and Laporte et al[27] where the weakened
456 AP2-arrestin and the phosphorylation-independent clathrin-arrestin interactions appear of
457 similar importance. The phosphorylation dependence of the AP2-arrestin interaction may also
458 play a role in modulating the strength of downstream arrestin-mediated signaling from
459 endosomes.[64,65] As such, the detailed understanding of these molecular interactions may provide
460 a framework for the development of novel therapeutics interfering with GPCR sequestration.
461

Methods

Constructs

The genes encoding full-length (arrestin2$^{1-418}$) and truncated (arrestin2$^{1-393}$) human arrestin2 constructs have been described before.[29] The arrestin2$^{\Delta CBL}$ construct in pET-28a (+) vector was obtained from the GenScript by replacing the loop residues of arrestin2 K357 to D385 with visual arrestin residues E365 to N376. The construct also contained an N-terminal hexahistidine tag for purification followed by a TEV cleavage site (ENLYFQG), resulting in the following total sequence (arrestin2$^{\Delta CBL}$ in bold, visual arrestin loop underlined):

MGSSHHHHHHSSGENLYFQG**MGDKGTRVFKKASPNGKLTVYLGKRDFVDHIDLVDPVDGVVLVDPEYLKERRVYVT**
LTCAFRYGREDLDVLGLTFRKDLFVANVQSFPPAPEDKKPLTRLQERLIKKLGEHAYPFTFEIPPNLPCSVTLQPG
PEDTGKACGVDYEVKAFLAENLEEKIHKRNSVRLVIRKVQYAPERPGPQPTAETTRQFLMSDKPLHLEASLDKEIY
YHGEPISVNVHVTNNTNKTVKKIKISVRQYADIVLFNTAQYKVPVAMEEADDTVAPSSTFSKVYTLTPFLANNREK
RGLALDGKLKHEDTNLASSTLLREGANREILGIIVSYKVKVKLVVSRGGLLGDLASSDVAVELPFTLMHPKPEDPA
KESYQDANIVFEDFARQRLKGMKDDKEEEEDGTGSPQLNNR

CLTC NTD (pETM33_CLTC_Clathrin propeller, Addgene plasmid #178471)[66] and AP2β2$^{701-937}$ (pETM33_AP2B1_adaptin, Addgene plasmid #178467)[66] were a gift from Ylva Ivarsson. Arrestin2-YFP was a gift from Robert Lefkowitz (Addgene plasmid # 36916).[67]

The arrestin2$^{\Delta LIELD}$-YFP construct was obtained from the arrestin2-YFP template by standard PCR reaction using KAPA HiFi polymerase (Forward primer: 5'-GAG ACT CCA GTA GAC ACC AAT ACC AAT GAT GAC GAC A-3'; Reverse primer: 5'-TGT CGT CAT CAT TGG TAT TGG TGT CTA CTG GAG TCT C-3').

Arrestin2^{R395A}-YFP was generated in the same manner using forward primer: 5’-GGA CTT TGC TCG TCA GGC GCT GAA AGG CAT GAA G-3’ and reverse primer: 5'-CTT CAT GCC TTT CAG CGC CTG ACG AGC AAA GTC C-3'.

The same protocol was applied for generating the arrestin2 $^{\Delta AP2}$-YFP clone with the forward primer of the sequence: 5'-GAC ACC AAT GAT GAC GCC ATT GTG GCT GAG GAC GCT GCT CGT CAG GCG CTG AAA GGC ATG-3' and reverse primer 5'-CAT GCC TTT CAG CGC CTG ACG AGC AGC GTC CTC AGC CAC AAT GGC GTC ATC ATT GGT GTC-3'.

490 The CCR5 construct in pcDNA3.1 used in cellular assays was obtained from GenScript. The
491 complete construct contained the full-length human CCR5 sequence (bold) followed by a GS-
492 linker and a C-terminal FLAG-tag (underlined):

493 **MDYQVSSPIYDINYYTSEPCQKINVKQIAARLLPPLYSLVFIFGFVGNMLVILILINCKRLKSMTDIYLLNLAISD**
494 **LFFLLTVPFWAHYAAAQWDFGNTMCQLLTGLYFIGFFSGIFFIILLTIDRYLAVVHAVFALKARTVTFGVVTSVIT**
495 **WVVAVFASLPGIIFTRSQKEGLHYTCSSHFPYSQYQFWKNFQTLKIVILGLVLPLLVMVICYSGILKTLLRCRNEK**
496 **KRHRAVRLIFTIMIVYFLFWAPYNIVLLLNTFQEFFGLNNCSSSNRLDQAMQVTETLGMTHCCINPIIYAFVGEKF**
497 **RNYLLVFFQKHIAKRFCKCCSIFQQEAPERASSVYTRSTGEQEISVGL**GSGGGGSGGSSSGGGGSGGSSSGGEFDY
498 KDDDDK

499 The genes encoding [5P12]CCL5,[68] CCL5[68] and [6P4]CCL5[69] for expression in *E. coli* have
500 been described previously.

501 **Protein expression and purification**

502 All protein constructs were expressed in *E. coli* BL21 (DE3) cultured in Lysogeny broth
503 medium (LB). For the preparation of the deuterated ^{15}N-labeled (and ^{13}C-labeled) NMR
504 samples, cells were grown in $D_2O/^{15}NH_4Cl$ (^{13}C-glucose) M9 minimal medium. For the
505 preparation of Ile-δ1-$^{13}CH_3$-labeled arrestin2$^{1-393}$, the minimal medium was supplemented with
506 80 mg per liter of 2-ketobutyric acid-4-^{13}C,3,3-d_2 sodium salt hydrate following previously
507 reported procedures.[70] In all cases, cells were grown at 37˚C until the optical density at 600 nm
508 ($OD_{600\ nm}$) reached 0.7–0.8. Thereafter protein expression was induced by the addition of 25 μM
509 isopropyl β-D-thiogalactopyranoside (IPTG) (arrestin2 constructs) or 1 mM IPTG (CLTC NTD
510 and AP2β2$^{701-937}$). The temperature was lowered to 18˚C (arrestin2 constructs) or 22˚C (CLTC
511 NTD and AP2β2$^{701-937}$) for an overnight expression, after which the cells were harvested by
512 centrifugation (30 min at 6000 rpm).

513 *Arrestin2*

514 The purification of arrestin2 has been described before.[29] In short, arrestin2$^{1-418}$, arrestin2^{1-}
515 ^{393}, arrestin2$^{\Delta CBL}$ and arrestin2$^{\Delta AP2}$ were purified on a Ni-NTA HiTrap HP column (GE Life
516 Sciences) and the His-tag was removed by overnight cleavage with TEV protease (homemade).
517 The cleaved protein was further separated from impurities by a reverse IMAC step on a Ni-NTA
518 HiTrap HP column. An ion exchange chromatography step using a 5-ml HiTrap Q HP anion

519 exchange column was then carried out before the final gel filtration step on a HiLoad 16/600
520 Superdex 200 pg gel filtration column (GE Healthcare) equilibrated with 20 mM HEPES,
521 150 mM NaCl, pH 7.4 (SEC buffer I). Protein purity was confirmed by SDS-PAGE.

522 *CLTC NTD*

523 CLTC NTD was purified similarly to the arrestin2 protocol using a Ni-NTA HiTrap HP
524 column. The His-tag was removed by overnight cleavage with 3C protease (homemade),
525 followed by a reverse IMAC step. The protein was concentrated in a Vivaspin 20 (Sartorius)
526 concentrator (10-kDa MWCO) before a final gel filtration step on a HiLoad 16/600 Superdex
527 S75 pg gel filtration column (GE Healthcare) equilibrated with SEC buffer I. Protein purity was
528 confirmed by SDS-PAGE.

529 *AP2β2*

530 AP2β2 was purified similarly to CLTC NTD. Due to a change of the isoelectric point from
531 6.6 to 7.7 after 3C protease cleavage, the pH of the SEC buffer was changed to 7.0 (SEC buffer
532 II, 20 mM HEPES, 150 mM NaCl, pH 7.0).

533 **Peptide synthesis**

534 Phosphorylated peptides (Supplementary Table 1) corresponding to the last 22 residues of
535 the human CCR5 receptor (CCR5pp3, CCR5pp4, CCR5pp6) were obtained from the Tufts
536 University Core Facility for peptide synthesis.

537 **Cell culture**

538 HeLa (ATCC CCL2) cells and HeLa KO cell line ($HeLa^{-arr2/3}$)[71] devoid of arrestin2 and
539 arrestin3 were grown in high-glucose Dulbecco's modified Eagle's medium (Sigma-Aldrich)
540 with 10% fetal bovine serum (FBS, Biowest), 2 mM L-glutamine (#25030; Gibco),
541 100 U ml^{-1} penicillin G and 100 ng ml^{-1} streptomycin (P433; Sigma-Aldrich Chemie GmbH),
542 1 mM sodium pyruvate (#S8636; Sigma-Aldrich Chemie GmbH) at 37˚C and 5% CO_2. For
543 transient cell transfections, cells were plated into six-well plates to reach 70% confluency the

544 following day and transfected with 0.3 μg of each arrestin2-YFP and CCR5 plasmid DNA
545 complexed with Helix-IN transfection reagent (OZ Biosciences).

546 **Immunostaining and microscopy**

547 In HeLa cell lines, arrestin2 and CCR5 were overexpressed by transiently transfecting
548 arrestin2-YFP and CCR5 respectively. CCR5 was stained with a primary FLAG antibody
549 (1:200, Thermo Fisher F3165) in 5% FBS in PBS. A secondary mouse (1:500) Alexa 633
550 (A21052, Invitrogen) antibody was used in 5% FBS in PBS. Fluoromount-G mounting medium
551 (Thermo Fischer) was used to mount the coverslips onto the imaging slide. Fluorescence and
552 DIC images were acquired with an ORCA-Flash 4.0 camera (Hamamatsu) mounted on an Axio
553 Imager.M2 fluorescence microscope with a 63x Plan-Apochromat objective (Carl Zeiss) and an
554 HXP 120C light source with ZEN 2.6 software. Image processing was performed using
555 OMERO.insight client,[72] and analyzed with Fiji software.[73]

556 To assess the recruitment of arrestin2 by CCR5, arrestin2-YFP- and CCR5-expressing cells
557 were incubated with 1 μM chemokine ligands. Individual coverslips were removed and fixed
558 with 4% PFA for 10 min at 0, 10, and 30 min post-ligand stimulation. Fixed cells were
559 permeabilized with 0.1% Triton X-100 in PBS for 5 min, rinsed with PBS twice and blocked
560 with 5% FBS in PBS. CCR5 was stained as mentioned previously and imaged. Colocalization
561 between arrestin2 and CCR5 was assessed by measuring the Mander's coefficient in 2-3 regions
562 of interest (ROI) of 100 μm^2 per cell using the Fiji JACOP plug-in.[74] The number of internalized
563 CCR5 puncta with and without arrestin2 was quantified manually by taking 3 ROIs of 100 μm^2
564 per cell using FiJi.

565 To image arrestin2/CCR5 trafficking to lysosome, arrestin2-YFP and CCR5 expressing cells
566 were treated with [6P4]CCL5. Individual coverslips were removed and fixed with 4% PFA for
567 10 min at 0, 10, and 30 min post stimulation. Fixed cells were permeabilized with 0.1% Triton
568 X-100 in PBS for 5 min, rinsed with PBS twice and blocked with 5% FBS in PBS. Lysosomes
569 were stained with LAMP1 antibody (1:200, Cell Signaling Technology, D2D11). CCR5 was

570 stained with FLAG antibody (1:200, Thermo Fisher F3165). Secondary rabbit (1:500) Alexa-
571 Fluor 568 (A110042 Invitrogen) and secondary mouse (1:500) Alexa-Fluor 633 (A21052,
572 Invitrogen) fluorescent antibodies were used respectively. Fixation, imaging and analysis was
573 performed as described above.

574 For assessing the effect of arrestin2 mutations, respective mutants were overexpressed with
575 CCR5 in HeLa$^{-arr2/3}$ and HeLa cells, followed by immunostaining and microscopy analysis as
576 described above (HeLa$^{-arr2/3}$: 60 min , HeLa: 30 min post [6P4]CCL5 stimulation).

577 **Live-cell imaging**

578 For live-cell imaging, Hela cells expressing arrestin2-YFP were seeded on an ibidi μ-slide
579 VI 0.4 channel slide (#80606, Ibidi), 24 hours prior to data acquisition. Live cell imaging was
580 performed in complete growth medium lacking phenol red at 37˚C with 5% CO_2 508 using an
581 inverted Axio Observer microscope (Zeiss) with a Plan Apochromat N 63x/1.40 oil DIC 509
582 M27 objective and a Photometrics Prime 95B camera. Filters with standard specifications for
583 GFP were used to image arrestin2-YFP. After selecting cells to be imaged, images were acquired
584 at 5 min intervals. Image processing was performed using OMERO.insight client,[72] and
585 analyzed with Fiji software.[73]

586 To image lysosome stained with lysotracker, Hela cells expressing arrestin2-YFP and CCR5
587 were seeded on an ibidi μ-slide VI 0.4 channel slide (#80606, Ibidi), 24 hours prior to data
588 acquisition. LysoTracker™ Deep Red (L12492) and peptide ligand was added in complete
589 growth medium lacking phenol red. Images were taken at 0 and 30 min timepoints.

590 **Statistics**

591 Statistical analysis was performed using GraphPad Prism 10.1.1 (GraphPad Software, Inc.,
592 San Diego, CA, USA). For statistical evaluation, the normality of the data was routinely tested
593 using the Shapiro-Wilk or Kolmogorov-Smirnov normality test. For the comparison of two
594 groups (Fig. 5a,b), a t-test was employed, whereas to compare three or more groups (Fig. 1d), a
595 one-way ANOVA was performed followed by a Kruskal-Wallis test.

596 **NMR Experiments**

597 NMR samples were prepared in SEC buffer I supplemented with 5% D_2O, 2 mM EDTA and
598 0.03% NaN_3 as 270-µl volumes in Shigemi tubes. The assignment sample contained 300 mM
599 NaCl. The spectra were recorded on a Bruker AVANCE 14.1 T (600 MHz) spectrometer
600 (arrestin2$^{1-393}$, AP2β2$^{701-937}$) or a Bruker AVANCE 21.2 T (900 MHz) spectrometer (CLTC
601 NTD) equipped with a TCI cryoprobe at 303 K. The spectra were processed with NMRPipe,[75]
602 assigned using CcpNmr AnalysisAssign[76] and analyzed with NMRFAM-SPARKY.[77]

603 *Arrestin2 assignment*

604 For the assignment of arrestin2 backbone resonances, HNCACB-TROSY, HNCA-TROSY
605 and HNCO-TROSY spectra were recorded on ^{15}N-, ^{13}C-, ^{2}H-labeled arrestin2$^{1-393}$ (100-150 µM)
606 samples.

607 *Arrestin2 titrations*

608 For detecting the CLTC NTD-arrestin2 interaction on arrestin2 by NMR, a titration of 50
609 µM ^{15}N-, ^{2}H-labeled arrestin2$^{1-393}$ with unlabeled CLTC NTD up to an equimolar amount was
610 monitored by ^{1}H-^{15}N HSQC-TROSY spectra recorded as 100 (^{15}N) x 512 (^{1}H) complex points
611 and acquisition times of 50 ms (^{15}N) and 55 ms (^{1}H) for 4.5 h. Peak intensities I were determined
612 by integration and the interaction was quantified relative to the intensity I_0 in the absence of
613 CLTC NTD. An intensity attenuation larger than one standard deviation of I/I_0 calculated from
614 all resonances was considered significant.

615 Similarly, a titration of 50 µM Ile-δ1-$^{13}CH_3$, ^{2}H-labeled arrestin2$^{1-393}$ with unlabeled CLTC
616 NTD up to a concentration of 600 µM was monitored by ^{1}H-^{13}C HMQC spectra recorded as 32
617 (^{13}C) x 512 (^{1}H) complex points and acquisition times of 20 ms (^{13}C) and 55 ms (^{1}H) for 1 h.
618 The assignments of the methyl groups were transferred from BMRB ID:51131.[50] K_D values
619 were obtained by nonlinear least-squares fitting using Matlab (Matlab_R2021b, MathWorks,
620 Inc.) and the following equation:

$$\Delta\delta = \Delta\delta_{max}\frac{[L] + [P] + K_D - \sqrt{([L] + [P] + K_D)^2 - 4[P][L]}}{2[P]} \quad (1)$$

621 where $\Delta\delta = \delta_{apo}-\delta_{bound}$ is the difference in the ^{13}C chemical shift, δ_{max} is the difference between
622 apo and the fully ligand-bound state, and [P] and [L] are the total protein (arrestin2) and ligand
623 (CLTC NTD) concentrations, respectively.

624 Chemical shift perturbations (CSP) were calculated from the relation:

$$\mathrm{CSP} = \sqrt{\Delta\delta_H{}^2 + \left(\frac{\Delta\delta_{13C}}{3.6}\right)^2} \quad (2)$$

625 where $\Delta\delta_H$ is the methyl proton chemical shift difference, and $\Delta\delta_{13C}$ is the ^{13}C-methyl chemical
626 shift difference between the apo and bound state. CSPs greater than one standard deviation from
627 the mean were considered significant.

628 *CLTC NTD titrations*

629 For detecting the CLTC NTD-arrestin2 interaction on CLTC NTD by NMR, a titration of
630 50 μM ^{15}N-, ^{2}H-labeled CLTC NTD with unlabeled arrestin2$^{1-393}$, arrestin2$^{1-418}$, arrestin2$^{\Delta CBL}$ or
631 arrestin2$^{1-393}$•CCR5pp6 up to an equimolar amount was monitored by ^{1}H-^{15}N HSQC-TROSY
632 spectra recorded as 100 (^{15}N) x 1024 (^{1}H) complex points and acquisition times of 35 ms (^{15}N)
633 and 80 ms (^{1}H) for 4.5 h. Assignments for CLTC NTD were transferred from BMRB
634 ID:25403.[51] Peak intensities were determined by quantifying peak volumes. Binding regions
635 were determined by intensity ratios as described above.

636 *AP2β2 titrations*

637 For detecting the AP2β2-arrestin2 interaction on AP2β2$^{701-937}$ by NMR, a titration of 50 μM
638 ^{15}N-, ^{2}H-labeled AP2β2$^{701-937}$ with unlabeled arrestin2$^{1-418}$ or arrestin2$^{1-418}$•CCR5pp6 up to an
639 equimolar amount was monitored by ^{1}H-^{15}N HSQC-TROSY spectra recorded as 100 (^{15}N) x
640 512 (^{1}H) complex points and acquisition times of 50 ms (^{15}N) and 55 ms (^{1}H) for 1 h.
641 Assignments for AP2β2$^{701-937}$ were transferred from BMRB ID: 52320.[56] Peak intensities were

642 determined by quantifying peak volumes. Binding regions were determined by intensity ratios
643 as described above.

644 **SEC binding assay**

645 SEC binding assays were performed on an UltiMate 3000 HPLC system. Samples
646 containing single polypeptides or their mixtures as indicated in the text and figure legends
647 (arrestin2$^{1-418}$: 10 μM, AP2β2: 10 μM, CLTC NTD: 10 μM, CCR5pp0: 100 μM, CCR5pp3: 100
648 μM, CCR5pp4: 100 μM, CCR5pp6: 25-100 μM) were prepared as 270 μL volumes in SEC
649 buffer II. Samples were injected with an autosampler using a 250-μL sample-loop onto a self-
650 packed 4.2-ml S200 10/300 SEC column (length 25 mm, diameter 4.6 mm), which had been
651 pre-equilibrated with SEC buffer II. Complex formation was monitored by following protein
652 absorbance at 280 nm at 2.6 ml elution volume and the composition of the respective SEC
653 fractions of all prepared complexes was analyzed by SDS-PAGE (Supplementary Fig. 6c).

654 The apparent dissociation constant of the arrestin2$^{1-418}$-AP2β2$^{701-937}$ complex in the presence
655 of the CCR5 phosphopeptides could be determined by integrating the SEC absorption peaks of
656 the complex and of the apo proteins and using their respective extinction coefficients. The
657 increase of absorbance around 2.6 ml is a consequence of the additional AP2β2$^{701-937}$ in that
658 elution region. This region overlaps to some extent with the elution profile of apo arrestin2$^{1-418}$.
659 Taking into account the 1:1 stoichiometry, the amount of formed complex was estimated by
660 integrating the profile between 2.4 and 2.8 ml, subtracting the respective integral of the apo
661 arrestin2$^{1-418}$ profile, and dividing the difference by the AP2β2$^{701-937}$ extinction coefficient.
662 Since the phosphopeptides do not contain tryptophan, their absorbance contribution was
663 ignored.

664 **Trypsin proteolysis**

665 Trypsin proteolysis assays were carried out by pre-incubating 100 μL of 20 μM arrestin2$^{1-418}$
666 and 100 μM CCR5pp6 or 500 μM CCR5pp4/CCR5pp3 phosphopeptide with 1- (CCR5pp6), 2-
667 (CCR5pp6) and 5-molar equivalents (CCR5pp6, CCR5pp4, CCR5pp3) of AP2β2 protein at

668 room temperature for 5-10 min in the SEC buffer II. Following pre-incubation, 1 ng of Trypsin
669 Gold (Promega) was added, and the mixture further incubated at 35 ˚C under gentle shaking
670 (500 rpm, ThermoMixer). Samples for SDS-PAGE (10 µL mixed with 10 µL of 4x SDS loading
671 buffer) were taken at 0, 5, 10, 20, 30, 60, and 90 min. The reaction was quenched by boiling the
672 samples for 10 min at 95˚C. Samples were then loaded on 4-20% precast gradient gels and
673 visualized with Instant Blue protein stain (Abcam). Control reactions were run with apo
674 arrestin2$^{1-418}$ and arrestin2$^{1-418}$ incubated with 100 µM CCR5pp6 or 60-500 µM
675 CCR5pp4/CCR5pp3 phosphopeptide.

676 SDS-PAGE gels were analyzed using ImageJ software[78] by integrating the peak area of the
677 two bands corresponding to the full length arrestin2$^{1-418}$ (top) and cleaved protein at residue
678 R393 (bottom). The relative abundance (in %) of arrestin2$^{1-418}$ was calculated from the
679 respective integrals at 5 min upon trypsin addition.

References

1. Hauser, A. S., Attwood, M. M., Rask-Andersen, M., Schiöth, H. B. & Gloriam, D. E. Trends in GPCR drug discovery: new agents, targets and indications. *Nat Rev Drug Discov* **16**, 829–842 (2017).
2. Weis, W. I. & Kobilka, B. K. The Molecular Basis of G Protein–Coupled Receptor Activation. *Annual Review of Biochemistry* **87**, 897–919 (2018).
3. Komolov, K. E. & Benovic, J. L. G protein-coupled receptor kinases: Past, present and future. *Cellular Signalling* **41**, 17–24 (2018).
4. Gurevich, V. V. & Gurevich, E. V. GPCR Signaling Regulation: The Role of GRKs and Arrestins. *Frontiers in Pharmacology* **10**, (2019).
5. Hanyaloglu, A. C. & Zastrow, M. von. Regulation of GPCRs by Endocytic Membrane Trafficking and Its Potential Implications. *Annu. Rev. Pharmacol. Toxicol.* **48**, 537–568 (2008).
6. Otero, C., Groettrup, M. & Legler, D. F. Opposite Fate of Endocytosed CCR7 and Its Ligands: Recycling versus Degradation1. *The Journal of Immunology* **177**, 2314–2323 (2006).
7. Gu, S. *et al.* Ligand-Dependent Mechanisms of C-C Chemokine Receptor 5 (CCR5) Trafficking Revealed by APEX2 Proximity Labeling Proteomics. 2023.11.01.565224 Preprint at https://doi.org/10.1101/2023.11.01.565224 (2023).
8. Wolfe, B. L. & Trejo, J. Clathrin-Dependent Mechanisms of G Protein-coupled Receptor Endocytosis. *Traffic* **8**, 462–470 (2007).
9. Kaksonen, M. & Roux, A. Mechanisms of clathrin-mediated endocytosis. *Nat Rev Mol Cell Biol* **19**, 313–326 (2018).
10. Smith, S. M. & Smith, C. J. Capturing the mechanics of clathrin-mediated endocytosis. *Current Opinion in Structural Biology* **75**, 102427 (2022).
11. Dell'Angelica, E. C. Clathrin-binding proteins: Got a motif? Join the network! *Trends in Cell Biology* **11**, 315–318 (2001).
12. Lemmon, S. K. & Traub, L. M. Getting in Touch with the Clathrin Terminal Domain. *Traffic* **13**, 511–519 (2012).
13. Smith, C. J., Grigorieff, N. & Pearse, B. M. F. Clathrin coats at 21 Å resolution: a cellular assembly designed to recycle multiple membrane receptors. *The EMBO Journal* **17**, 4943–4953 (1998).
14. Popova, N. V., Deyev, I. E. & Petrenko, A. G. Clathrin-Mediated Endocytosis and Adaptor Proteins. *Acta Naturae* **5**, 62–73 (2013).
15. Kovtun, O., Dickson, V. K., Kelly, B. T., Owen, D. J. & Briggs, J. A. G. Architecture of the AP2/clathrin coat on the membranes of clathrin-coated vesicles. *Science Advances* **6**, eaba8381 (2020).
16. Kelly, B. T. *et al.* AP2 controls clathrin polymerization with a membrane-activated switch. *Science* **345**, 459–463 (2014).
17. Schmid, E. M. *et al.* Role of the AP2 β-Appendage Hub in Recruiting Partners for Clathrin-Coated Vesicle Assembly. *PLOS Biology* **4**, e262 (2006).
18. Collins, B. M., McCoy, A. J., Kent, H. M., Evans, P. R. & Owen, D. J. Molecular Architecture and Functional Model of the Endocytic AP2 Complex. *Cell* **109**, 523–535 (2002).
19. Smith, S. M., Baker, M., Halebian, M. & Smith, C. J. Weak Molecular Interactions in Clathrin-Mediated Endocytosis. *Frontiers in Molecular Biosciences* **4**, (2017).
20. Jackson, L. P. *et al.* A Large-Scale Conformational Change Couples Membrane Recruitment to Cargo Binding in the AP2 Clathrin Adaptor Complex. *Cell* **141**, 1220–1229 (2010).
21. Paing, M. M., Johnston, C. A., Siderovski, D. P. & Trejo, J. Clathrin Adaptor AP2 Regulates Thrombin Receptor Constitutive Internalization and Endothelial Cell Resensitization. *Molecular and Cellular Biology* **26**, 3231–3242 (2006).
22. Marchese, A., Paing, M. M., Temple, B. R. S. & Trejo, J. G Protein–Coupled Receptor Sorting to Endosomes and Lysosomes. *Annual Review of Pharmacology and Toxicology* **48**, 601–629 (2008).
23. Goodman, O. B. *et al.* β-Arrestin acts as a clathrin adaptor in endocytosis of the β2-adrenergic receptor. *Nature* **383**, 447–450 (1996).
24. Lefkowitz, R. J. & Shenoy, S. K. Transduction of Receptor Signals by ß-Arrestins. *Science* **308**, 512–517 (2005).
25. Goodman, O. B., Krupnick, J. G., Gurevich, V. V., Benovic, J. L. & Keen, J. H. Arrestin/Clathrin Interaction: LOCALIZATION OF THE ARRESTIN BINDING LOCUS TO THE CLATHRIN TERMINAL DOMAIN*. *Journal of Biological Chemistry* **272**, 15017–15022 (1997).
26. Krupnick, J. G., Goodman, O. B., Keen, J. H. & Benovic, J. L. Arrestin/Clathrin Interaction: LOCALIZATION OF THE CLATHRIN BINDING DOMAIN OF NONVISUAL ARRESTINS TO THE CARBOXYL TERMINUS*. *Journal of Biological Chemistry* **272**, 15011–15016 (1997).
27. Laporte, S. A., Oakley, R. H., Holt, J. A., Barak, L. S. & Caron, M. G. The Interaction of β-Arrestin with the AP-2 Adaptor Is Required for the Clustering of β2-Adrenergic Receptor into Clathrin-coated Pits*. *Journal of Biological Chemistry* **275**, 23120–23126 (2000).

28. Oakley, R. H., Laporte, S. A., Holt, J. A., Caron, M. G. & Barak, L. S. Differential Affinities of Visual Arrestin, βArrestin1, and βArrestin2 for G Protein-coupled Receptors Delineate Two Major Classes of Receptors*. *Journal of Biological Chemistry* **275**, 17201–17210 (2000).
29. Isaikina, P. *et al.* A key GPCR phosphorylation motif discovered in arrestin2·CCR5 phosphopeptide complexes. *Molecular Cell* **83**, 2108-2121.e7 (2023).
30. Alkhatib, G. The biology of CCR5 and CXCR4. *Current Opinion in HIV and AIDS* **4**, 96–103 (2009).
31. Zeng, Z., Lan, T., Wei, Y. & Wei, X. CCL5/CCR5 axis in human diseases and related treatments. *Genes & Diseases* **9**, 12–27 (2022).
32. Patterson, B. K. *et al.* CCR5 inhibition in critical COVID-19 patients decreases inflammatory cytokines, increases CD8 T-cells, and decreases SARS-CoV2 RNA in plasma by day 14. *International Journal of Infectious Diseases* **103**, 25–32 (2021).
33. Jiao, X. *et al.* Recent Advances Targeting CCR5 for Cancer and Its Role in Immuno-Oncology. *Cancer Res* **79**, 4801–4807 (2019).
34. Maharana, J. *et al.* Structural snapshots uncover a key phosphorylation motif in GPCRs driving β-arrestin activation. *Molecular Cell* **83**, 2091-2107.e7 (2023).
35. Huang, W. *et al.* Structure of the neurotensin receptor 1 in complex with β-arrestin 1. *Nature* **579**, 303–308 (2020).
36. Bous, J. *et al.* Structure of the vasopressin hormone-V2 receptor-β-arrestin1 ternary complex. *Sci Adv* **8**, eabo7761 (2022).
37. Kang, Y. *et al.* Crystal structure of rhodopsin bound to arrestin by femtosecond X-ray laser. *Nature* **523**, 561–567 (2015).
38. Oakley, R. H., Laporte, S. A., Holt, J. A., Barak, L. S. & Caron, M. G. Molecular Determinants Underlying the Formation of Stable Intracellular G Protein-coupled Receptor-β-Arrestin Complexes after Receptor Endocytosis*. *Journal of Biological Chemistry* **276**, 19452–19460 (2001).
39. Signoret, N. *et al.* Agonist-induced Endocytosis of CC Chemokine Receptor 5 Is Clathrin Dependent. *Mol Biol Cell* **16**, 902–917 (2005).
40. Fraile-Ramos, A., Kohout, T. A., Waldhoer, M. & Marsh, M. Endocytosis of the Viral Chemokine Receptor US28 Does Not Require Beta-Arrestins But Is Dependent on the Clathrin-Mediated Pathway. *Traffic* **4**, 243–253 (2003).
41. Gaertner, H. *et al.* Highly potent, fully recombinant anti-HIV chemokines: Reengineering a low-cost microbicide. *PNAS* **105**, 17706–17711 (2008).
42. Hughes, C. E. & Nibbs, R. J. B. A guide to chemokines and their receptors. *The FEBS Journal* **285**, 2944–2971 (2018).
43. Isaikina, P. *et al.* Structural basis of the activation of the CC chemokine receptor 5 by a chemokine agonist. *Science Advances* (2021) doi:10.1126/sciadv.abg8685.
44. Beautrait, A. *et al.* A new inhibitor of the β-arrestin/AP2 endocytic complex reveals interplay between GPCR internalization and signalling. *Nat Commun* **8**, 15054 (2017).
45. Martins, E. *et al.* Arrestin Recruitment to C-C Chemokine Receptor 5: Potent C-C Chemokine Ligand 5 Analogs Reveal Differences in Dependence on Receptor Phosphorylation and Isoform-Specific Recruitment Bias. *Mol Pharmacol* **98**, 599–611 (2020).
46. Mueller, A., Kelly, E. & Strange, P. G. Pathways for internalization and recycling of the chemokine receptor CCR5. *Blood* **99**, 785–791 (2002).
47. Kang, D. S. *et al.* Structure of an Arrestin2-Clathrin Complex Reveals a Novel Clathrin Binding Domain That Modulates Receptor Trafficking. *J Biol Chem* **284**, 29860–29872 (2009).
48. Jumper, J. *et al.* Highly accurate protein structure prediction with AlphaFold. *Nature* **596**, 583–589 (2021).
49. Tugarinov, V., Hwang, P. M., Ollerenshaw, J. E. & Kay, L. E. Cross-Correlated Relaxation Enhanced 1H−13C NMR Spectroscopy of Methyl Groups in Very High Molecular Weight Proteins and Protein Complexes. *J. Am. Chem. Soc.* **125**, 10420–10428 (2003).
50. Shiraishi, Y. *et al.* Biphasic activation of β-arrestin 1 upon interaction with a GPCR revealed by methyl-TROSY NMR. *Nat Commun* **12**, 7158 (2021).
51. Zhuo, Y. *et al.* Nuclear Magnetic Resonance Structural Mapping Reveals Promiscuous Interactions between Clathrin-Box Motif Sequences and the N-Terminal Domain of the Clathrin Heavy Chain. *Biochemistry* **54**, 2571–2580 (2015).
52. Kern, R. C., Kang, D. S. & Benovic, J. L. Arrestin2/Clathrin Interaction Is Regulated by Key N- and C-Terminal Regions in Arrestin2. *Biochemistry* **48**, 7190–7200 (2009).
53. Laporte, S. A., Miller, W. E., Kim, K.-M. & Caron, M. G. β-Arrestin/AP-2 Interaction in G Protein-coupled Receptor Internalization: IDENTIFICATION OF A β-ARRESTIN BINDING SITE IN β2-ADAPTIN*. *Journal of Biological Chemistry* **277**, 9247–9254 (2002).
54. Kim, Y.-M. & Benovic, J. L. Differential Roles of Arrestin-2 Interaction with Clathrin and Adaptor Protein 2 in G Protein-coupled Receptor Trafficking*. *Journal of Biological Chemistry* **277**, 30760–30768 (2002).
55. Moaven, H. *et al.* Visual arrestin interaction with clathrin adaptor AP-2 regulates photoreceptor survival in the vertebrate retina. *Proceedings of the National Academy of Sciences* **110**, 9463–9468 (2013).

56. Naudi-Fabra, S. *et al.* An extended interaction site determines binding between AP180 and AP2 in clathrin mediated endocytosis. *Nat Commun* **15**, 5884 (2024).
57. Xiao, K., Shenoy, S. K., Nobles, K. & Lefkowitz, R. J. Activation-dependent Conformational Changes in β-Arrestin 2*. *Journal of Biological Chemistry* **279**, 55744–55753 (2004).
58. Barsi-Rhyne, B., Manglik, A. & von Zastrow, M. Discrete GPCR-triggered endocytic modes enable β-arrestins to flexibly regulate cell signaling. *eLife* **11**, e81563 (2022).
59. Escola, J.-M., Kuenzi, G., Gaertner, H., Foti, M. & Hartley, O. CC Chemokine Receptor 5 (CCR5) Desensitization: CYCLING RECEPTORS ACCUMULATE IN THE TRANS-GOLGI NETWORK*. *Journal of Biological Chemistry* **285**, 41772–41780 (2010).
60. Ariel, A. *et al.* Apoptotic neutrophils and T cells sequester chemokines during immune response resolution through modulation of CCR5 expression. *Nat Immunol* **7**, 1209–1216 (2006).
61. Lally, C. C. M., Bauer, B., Selent, J. & Sommer, M. E. C-edge loops of arrestin function as a membrane anchor. *Nat Commun* **8**, 14258 (2017).
62. Janetzko, J. *et al.* Membrane phosphoinositides regulate GPCR-β-arrestin complex assembly and dynamics. *Cell* **185**, 4560-4573.e19 (2022).
63. Grimes, J. *et al.* Plasma membrane preassociation drives β-arrestin coupling to receptors and activation. *Cell* **186**, 2238-2255.e20 (2023).
64. Tohgo, A. *et al.* The Stability of the G Protein-coupled Receptor-β-Arrestin Interaction Determines the Mechanism and Functional Consequence of ERK Activation *. *Journal of Biological Chemistry* **278**, 6258–6267 (2003).
65. Jean-Charles, P.-Y., Kaur, S. & Shenoy, S. K. G Protein–Coupled Receptor Signaling Through β-Arrestin–Dependent Mechanisms. *Journal of Cardiovascular Pharmacology* **70**, 142 (2017).
66. Benz, C. *et al.* Proteome-scale mapping of binding sites in the unstructured regions of the human proteome. *Molecular Systems Biology* **18**, e10584 (2022).
67. Violin, J. D., Ren, X.-R. & Lefkowitz, R. J. G-protein-coupled receptor kinase specificity for beta-arrestin recruitment to the beta2-adrenergic receptor revealed by fluorescence resonance energy transfer. *J Biol Chem* **281**, 20577–20588 (2006).
68. Wiktor, M., Hartley, O. & Grzesiek, S. Characterization of Structure, Dynamics, and Detergent Interactions of the Anti-HIV Chemokine Variant 5P12-RANTES. *Biophysical Journal* **105**, 2586–2597 (2013).
69. Isaikina, P. *et al.* Chapter 6 - Preparation of a stable CCL5·CCR5·Gi signaling complex for Cryo-EM analysis. in *Methods in Cell Biology* (ed. Shukla, A. K.) vol. 169 115–141 (Academic Press, 2022).
70. Tugarinov, V., Kanelis, V. & Kay, L. E. Isotope labeling strategies for the study of high-molecular-weight proteins by solution NMR spectroscopy. *Nat Protoc* **1**, 749–754 (2006).
71. D'Agostino, G. *et al.* β-Arrestin1 and β-Arrestin2 Are Required to Support the Activity of the CXCL12/HMGB1 Heterocomplex on CXCR4. *Front Immunol* **11**, 550824 (2020).
72. Allan, C. *et al.* OMERO: flexible, model-driven data management for experimental biology. *Nat Methods* **9**, 245–253 (2012).
73. Schindelin, J. *et al.* Fiji: an open-source platform for biological-image analysis. *Nat Methods* **9**, 676–682 (2012).
74. Bolte, S. & Cordelières, F. P. A guided tour into subcellular colocalization analysis in light microscopy. *Journal of Microscopy* **224**, 213–232 (2006).
75. Delaglio, F. *et al.* NMRPipe: A multidimensional spectral processing system based on UNIX pipes. *J Biomol NMR* **6**, 277–293 (1995).
76. Skinner, S. P. *et al.* CcpNmr AnalysisAssign: a flexible platform for integrated NMR analysis. *J Biomol NMR* **66**, 111–124 (2016).
77. Lee, W., Tonelli, M. & Markley, J. L. NMRFAM-SPARKY: enhanced software for biomolecular NMR spectroscopy. *Bioinformatics* **31**, 1325–1327 (2015).
78. Schneider, C. A., Rasband, W. S. & Eliceiri, K. W. NIH Image to ImageJ: 25 years of image analysis. *Nat Methods* **9**, 671–675 (2012).

Acknowledgments

We gratefully acknowledge I. Hertel and M. Rogowski for the expression and purification of proteases and CCL5 ligands. We thank Prof. Mariagrazia Uguccioni and Dr. Valentina Cecchinato (Institute for Research in Biomedicine, Bellinzona, Switzerland) for the HeLa$^{-arr2/3}$ cells. This work was supported by the Swiss National Science Foundation (grants 31-201270 and IZLIZ3-200298 to S.G., 31-197779 and 31-185127 to A.S.), and by a Fellowship for Excellence by the Biozentrum Basel International PhD Program to I.P.

Author contributions

I.P., S.D., P.I., A.S., and S.G. conceived the study. I.P. and L.A.A generated all the constructs and mutants for the cellular assays. S.D. performed the cellular assays and analyzed the cellular data with guidance from A.S. I.P. expressed and purified proteins. I.P. recorded NMR experiments and analyzed NMR data. I.P. designed and analyzed SEC and trypsin proteolysis assay. I.P. and S.G. wrote the manuscript with inputs from all co-authors.

Competing interest

The authors declare that they have no competing interests.

Data and materials availability

All data needed to evaluate the conclusions in the paper are present in the main text and/or Supplementary information.

869 **Figures**

870 **Fig. 1: CCR5 internalization in the presence of the chemokine ligands.** CCR5 internalization
871 monitored in HeLa cells co-transfected with plasmids containing arrestin2-YFP (green) and
872 CCR5 genes (magenta) stimulated with **a**, [5P12]CCL5 (antagonist) **b**, CCL5 (natural agonist)
873 **c**, [6P4]CCL5 (super-agonist). Cells were stimulated for 0, 10, and 30 min with chemokine
874 ligands before fixation and preparation for fluorescence microscopy. Each image is
875 accompanied by a zoomed region of interest (white squares) showing deconvolved CCR5 and
876 arrestin2-YFP signals. **d**, Mander's colocalization coefficients of the CCR5 and arrestin2-YFP
877 signals in the absence and presence of chemokine ligands 30 min after stimulation. Individual
878 values, as well as mean and standard deviation are shown for N=3 biological replicates and n=45
879 ROIs from 20 cells; ****: $P < 0.0001$; ns: not significant ($P > 0.9999$). **e** Number of CCR5-
880 positive ($CCR5^+$) and CCR5/arrestin2-positive ($CCR5^+$/$arrestin2^+$) puncta after 30 min
881 [6P4]CCL5 ligand stimulation. Individual values, as well as mean and standard deviation are
882 shown for N=3 biological replicates and n=90 ROIs from 30 cells; ns: not significant ($P >$
883 0.9999). **f**, CCR5 and arrestin2 fluorescence signals along the trajectory from the plasma
884 membrane to the nucleus (blue line in panel **c**) 30 min after [6P4]CCL5 ligand stimulation. **g**,
885 Lysosomal trafficking of the CCR5 (magenta) and arrestin2 (cyan) complex in presence of the
886 [6P4]CCL5 monitored in the HeLa cells using LAMP1 antibodies (yellow). No recruitment to
887 the lysosome is observed.

888 **Fig. 2: Arrestin2-CLTC NTD interactions detected by arrestin2 NMR spectra. a**,
889 AlphaFold2 model of $Arrestin2^{1-418}$ showing the N- and C-domain (gray) followed by the
890 clathrin-binding loop (CBL, orange), C-terminal β20 strand (yellow) and the disordered C-
891 terminal tail (blue). The C-terminal strand β20 forms a parallel β-sheet with the N-terminal
892 strand β1 (pink) of inactive arrestin2 and is released from the arrestin2 upon activation by
893 phosphopeptides. Arrestin2 residues interacting with CLTC NTD are shown as green (red for
894 main interacting residue I377) spheres. The clathrin and AP2 binding motifs are indicated in the
895 arrestin2 sequence on the top. **b**, Part of ^1H-^{15}N TROSY spectrum of apo $arrestin2^{1-393}$ (black)
896 and upon addition of an equimolar amount of CLTC NTD (green). Assigned CBL $arrestin2^{1-393}$
897 residues are indicated. **c**, Intensity ratios of assigned complexed vs. apo $arrestin2^{1-393}$ CBL
898 resonances. The region between T374 and T381 undergoes significant intensity attenuation. **d**,
899 ^1H-^{13}C HMQC spectra of apo Ile-δ1-$^{13}CH_3$, ^2H-labeled $arrestin2^{1-393}$ (black) and upon addition
900 of an equimolar amount of the CLTC NTD (green). **e**, Intensity attenuation (top) and chemical
901 shift perturbation (bottom) of $arrestin2^{1-393}$ isoleucine $^1H_3$-$^{13}C^{\delta 1}$ resonances upon CLTC NTD
902 addition. Out of 15 isoleucine residues, significant changes are observed only for I377. **f**, Left:

903 part of ^{1}H-^{13}C HMQC spectrum showing resonance shifts of I377 upon CLTC NTD binding.
904 Right: detected chemical shift changes as a function of CLTC NTD concentration. The solid
905 line depicts a global non-linear least-square fit to the data points with respective dissociation
906 constant.
907 **Fig. 3: Arrestin2-CLTC NTD interactions detected by CLTC NTD NMR spectra.** (Left):
908 intensity attenuation I/I_0 of CLTC NTD ^{1}H-^{15}N TROSY resonances upon addition of equimolar
909 amounts of various arrestin2 constructs: **a**, apo arrestin2$^{1-393}$ **b**, CCR5pp6-activated arrestin2$^{1-393}$
910 **c**, full-length arrestin2$^{1-418}$ **d**, arrestin2$^{\Delta CBL}$ with removed clathrin-binding motif. Regions that
911 undergo significant attenuation upon interaction with arrestin2 are indicated by arrows. Right:
912 residues undergoing significant intensity attenuation (one standard deviation below the average
913 signal attenuation) are marked on the structure of CLTC NTD (PDB: 3GD1) together with a
914 schematic representation of the respective arrestin2 construct.
915 **Fig. 4: Arrestin2 interaction with the C-terminal domain of the AP2β2. a**, Structure of
916 AP2β2$^{701-937}$ (orange) in complex with arrestin C-terminal peptide (blue) (PDB: 2IV8).
917 Important residues from both chains stabilizing the interaction are depicted in stick
918 representation. **b-f** SEC profiles of arrestin2$^{1-418}$, AP2β2$^{701-937}$, various phosphopeptides and
919 their mixtures. The annotated color coding below the SEC profile indicates the individual
920 sample composition. In panels **b, c, e,** 'mixture' refers to a SEC sample containing all of the
921 individual components indicated on the left. In panels **d, f**, the primary sample composition is
922 indicated above the SEC profile, and the annotated color coding below the SEC profile indicates
923 the added component to the primary sample composition. **g**, Apparent affinities of the
924 complexes derived by integrating the SEC peaks marked in Fig. 4f and scaling the integrals by
925 the respective extinction coefficients. 'nd' indicates 'not detected'. **h, i** (Left): intensity
926 attenuation I/I_0 of AP2β2$^{701-937}$ ^{1}H-^{15}N TROSY resonances upon addition of equimolar amounts
927 of apo arrestin2$^{1-418}$ (**h**) or CCR5pp6-activated arrestin2$^{1-418}$ (**i**). Regions that undergo significant
928 attenuation upon interaction with arrestin2 are indicated by arrows. Right: residues undergoing
929 significant intensity attenuation are marked on the structure of AP2β2 (PDB: 2IV8) together
930 with a schematic representation of the respective arrestin2 construct.
931 **Fig. 5: Dependence of CCR5 internalization on arrestin2 interactions with clathrin or AP2**
932 **monitored in HeLa$^{-arr2/3}$ cells. a,** CCR5 internalization induced by 60 min [6P4]CCL5 ligand
933 stimulation in HeLa cells co-transfected with plasmids containing CCR5 and arrestin2-YFP,
934 arrestin2-YFP$^{\Delta LIELD}$, arrestin2-YFP^{R395A}, arrestin2-YFP$^{\Delta AP2}$ or empty pcDNA3.1. **b**, **c,**
935 Internalization quantified by counting the number of puncta (**b**) positive for CCR5 and arrestin2
936 (CCR5^{+}/arrestin2^{+}) or (**c**) only CCR5^{+} 60 min after ligand stimulation in the HeLa$^{-arr2/3}$ cells. No

937 significant difference in CCR5 internalization is detected for the arrestin2-YFP$^{\Delta LIELD}$ and
938 arrestin2-YFP^{R395A} constructs (ns, not significant: $P > 0.9999$) whereas the absence of the AP2
939 binding motif in the arrestin2$^{\Delta AP2}$-YFP construct causes a significant (****: $P < 0.0001$)
940 reduction of CCR5 internalization 60 min after ligand incubation. Mean and standard deviation
941 are shown for N=3 biological replicates and n=90 ROIs from 30 cells.
942 **Fig. 6: Overall scheme of arr-class A and b GPCR internalization.** Schematic difference of
943 arrestin2-mediated internalization of arr-class B (left) vs. arr-class A (right) GPCRs. Arr-class
944 B GPCRs bind stably to arrestin due to their high levels of phosphorylation. This results in a
945 robust release of the arrestin C-terminus, a stable interaction with AP2 and formation of a long-
946 lived GPCR•arrestin complex. Arr-class A GPCRs bind weakly to arrestin due to their poor
947 phosphorylation. They require stabilization of the arrestin complex by membrane-bound PIP_2
948 molecules. The arrestin C-terminus is not fully released and consequently the interaction with
949 AP2 is unstable.

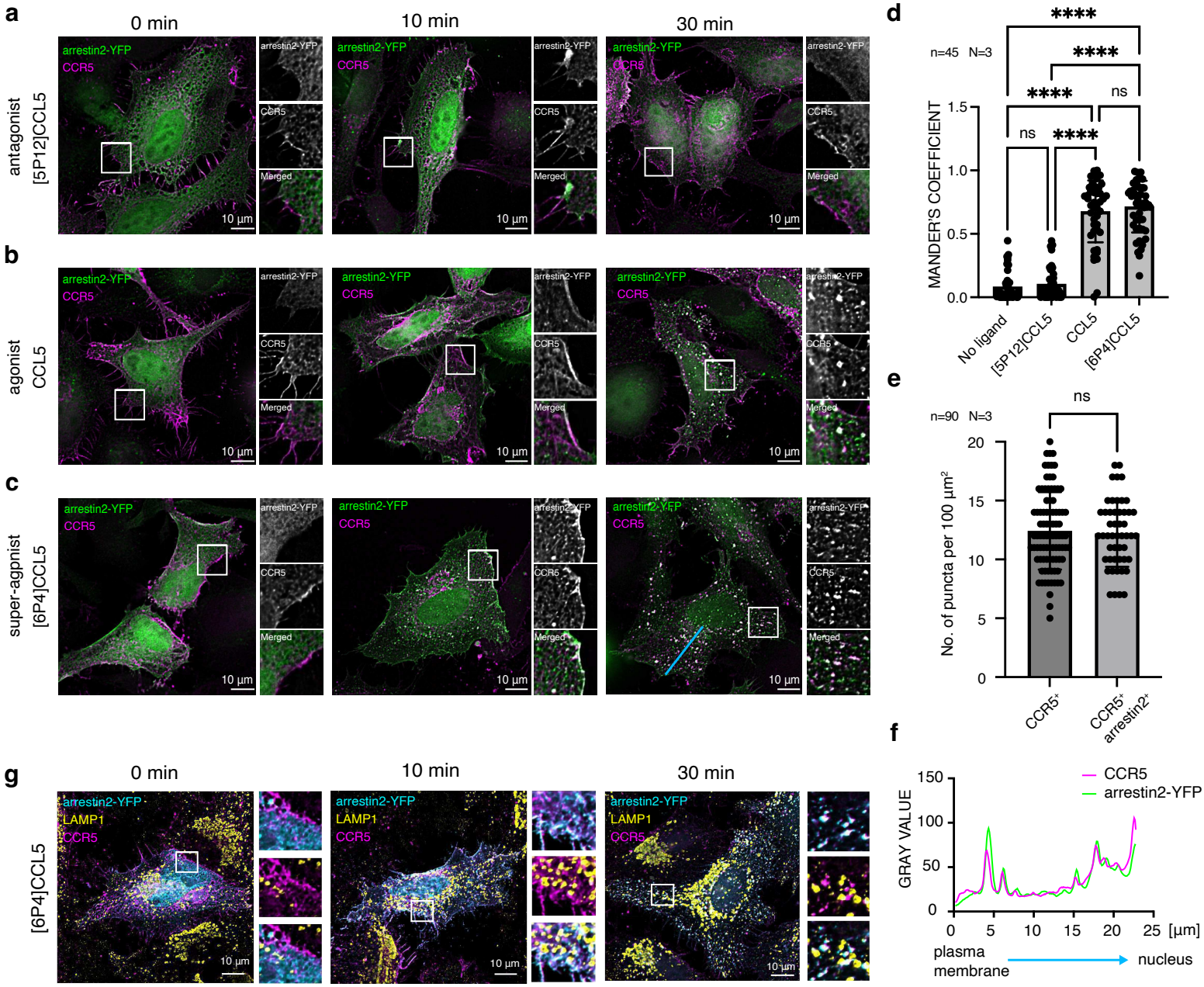
a
0 min
10 min
30 min
antagonist
[5P12]CCL5
arrestin2-YFP
CCR5
Merged
10 µm
b
agonist
CCL5
c
super-agpnist
[6P4]CCL5
d
n=45 N=3
MANDER'S COEFFICIENT
1.5
1.0
0.5
0.0
****
ns
No ligand
[5P12]CCL5
CCL5
[6P4]CCL5
e
n=90 N=3
No. of puncta per 100 µm²
20
15
10
5
0
CCR5⁺
CCR5⁺ arrestin2⁺
f
GRAY VALUE
150
100
50
0
CCR5
arrestin2-YFP
0
5
10
15
20
25
[µm]
plasma membrane
nucleus
g
LAMP1

Figure 1

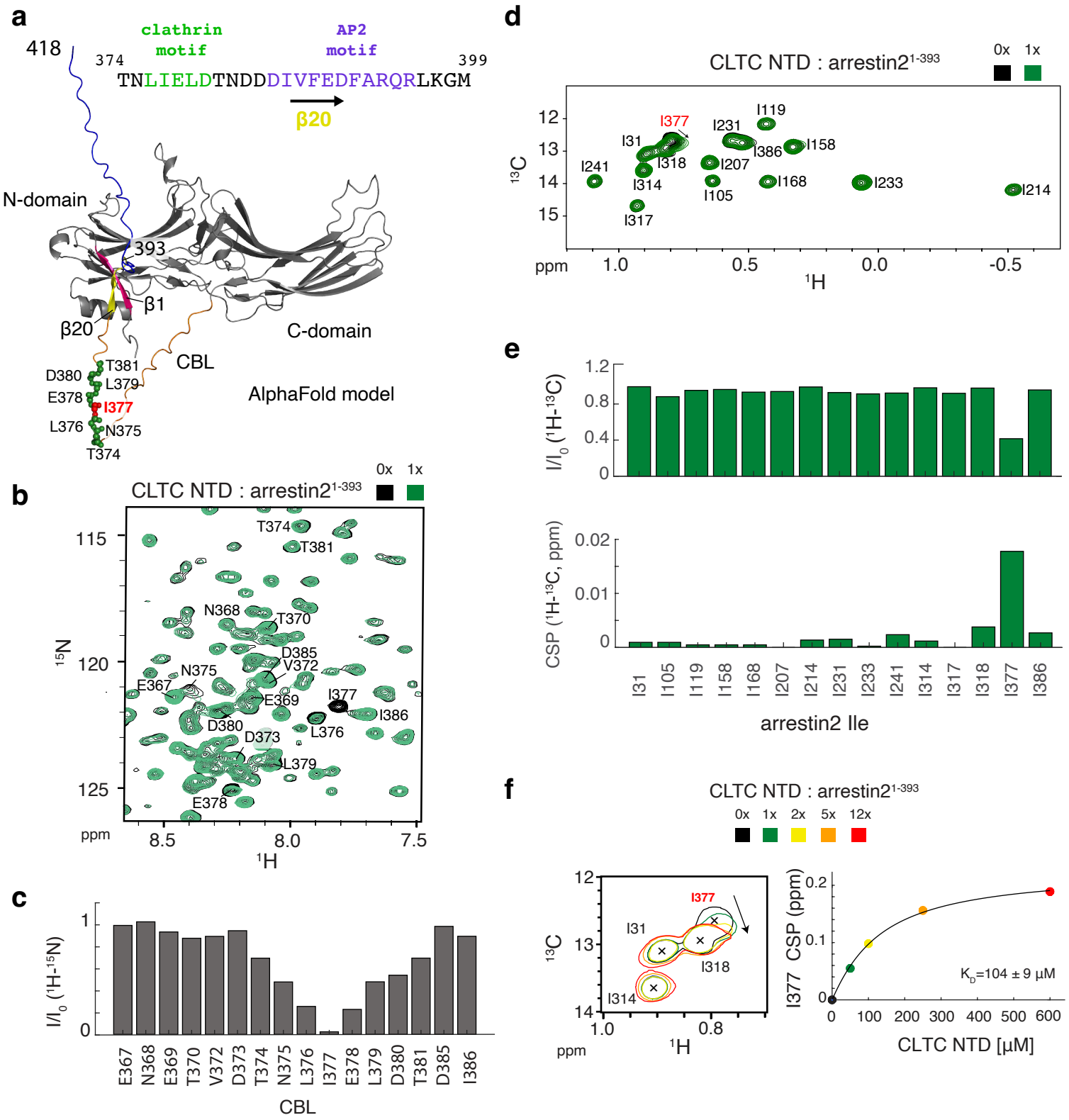
a
418
374
clathrin motif
AP2 motif
399
TNLIELDTNDDDIVFEDFARQRLKGM
β20
N-domain
393
β1
β20
C-domain
CBL
T381
D380
L379
E378
I377
L376
N375
T374
AlphaFold model
b
CLTC NTD : arrestin2 1-393
0x 1x
115
120
125
15N
ppm
8.5
8.0
7.5
1H
T374
T381
N368
T370
D385
V372
N375
E367
E369
I377
I386
D380
L376
D373
L379
E378
c
I/I0 (1H-15N)
1
0
E367 N368 E369 T370 V372 D373 T374 N375 L376 I377 E378 L379 D380 T381 D385 I386
CBL
d
CLTC NTD : arrestin2 1-393
0x 1x
12
13
14
15
13C
ppm
1.0
0.5
0.0
-0.5
1H
I377
I119
I231
I31
I158
I386
I318
I207
I241
I314
I168
I233
I214
I105
I317
e
I/I0 (1H-13C)
1.2
0.8
0.4
0
CSP (1H-13C, ppm)
0.02
0.01
0
I31 I105 I119 I158 I168 I207 I214 I231 I233 I241 I314 I317 I318 I377 I386
arrestin2 Ile
f
CLTC NTD : arrestin2 1-393
0x 1x 2x 5x 12x
12
13
14
13C
I377
I31
I318
I314
1.0
0.8
ppm
1H
I377 CSP (ppm)
0.2
0.1
0
KD=104 ± 9 μM
0 100 200 300 400 500 600
CLTC NTD [μM]

Figure 2

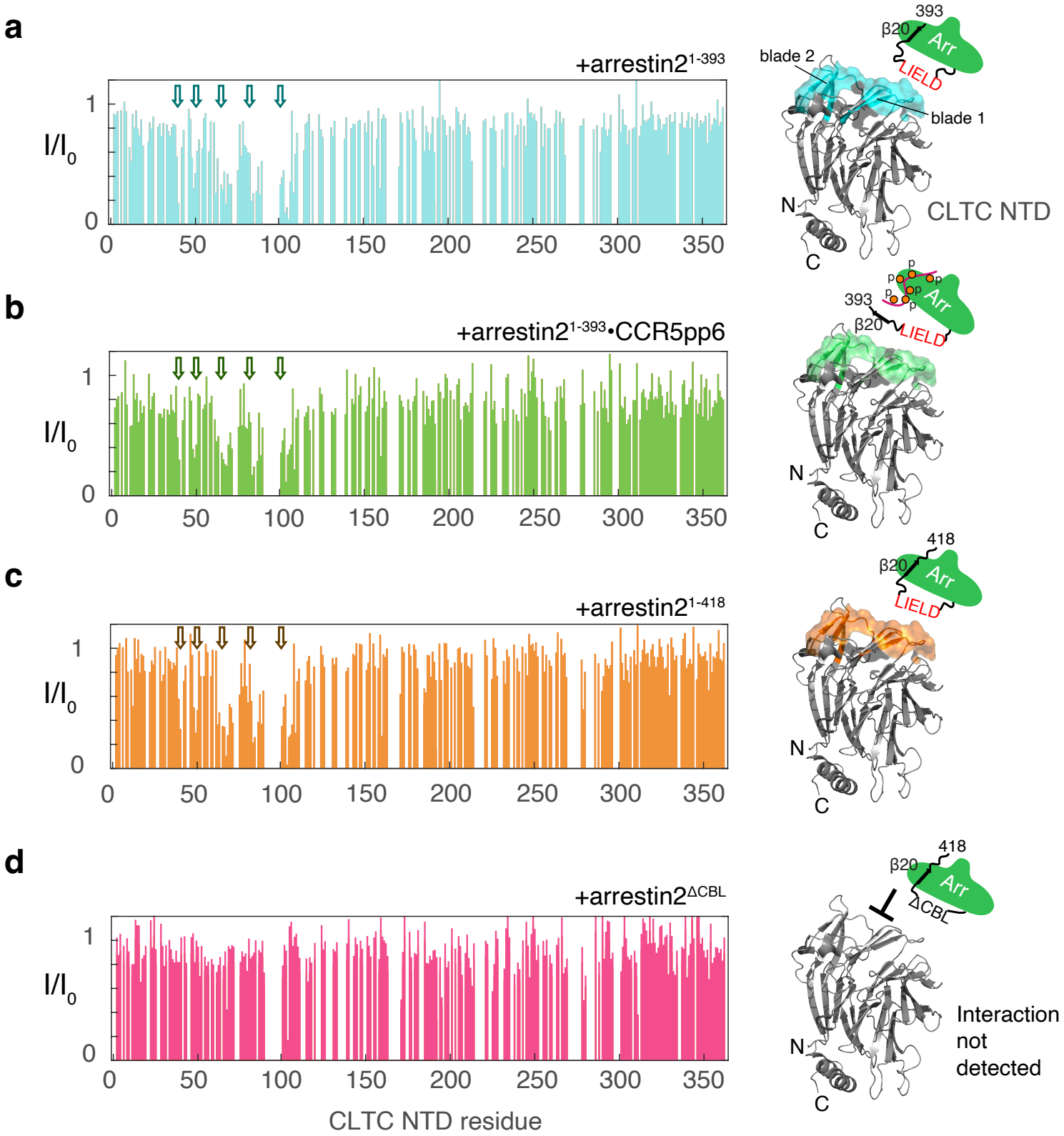
a
+arrestin2$^{1-393}$
I/I$_0$
1
0
0
50
100
150
200
250
300
350
393
β20
Arr
LIELD
blade 2
blade 1
N
C
CLTC NTD
b
+arrestin2$^{1-393}$•CCR5pp6
I/I$_0$
1
0
0
50
100
150
200
250
300
350
p
393
β20
Arr
LIELD
N
C
c
+arrestin2$^{1-418}$
I/I$_0$
1
0
0
50
100
150
200
250
300
350
418
β20
Arr
LIELD
N
C
d
+arrestin2$^{\Delta CBL}$
I/I$_0$
1
0
0
50
100
150
200
250
300
350
CLTC NTD residue
418
β20
Arr
ΔCBL
N
C
Interaction
not
detected

Figure 3

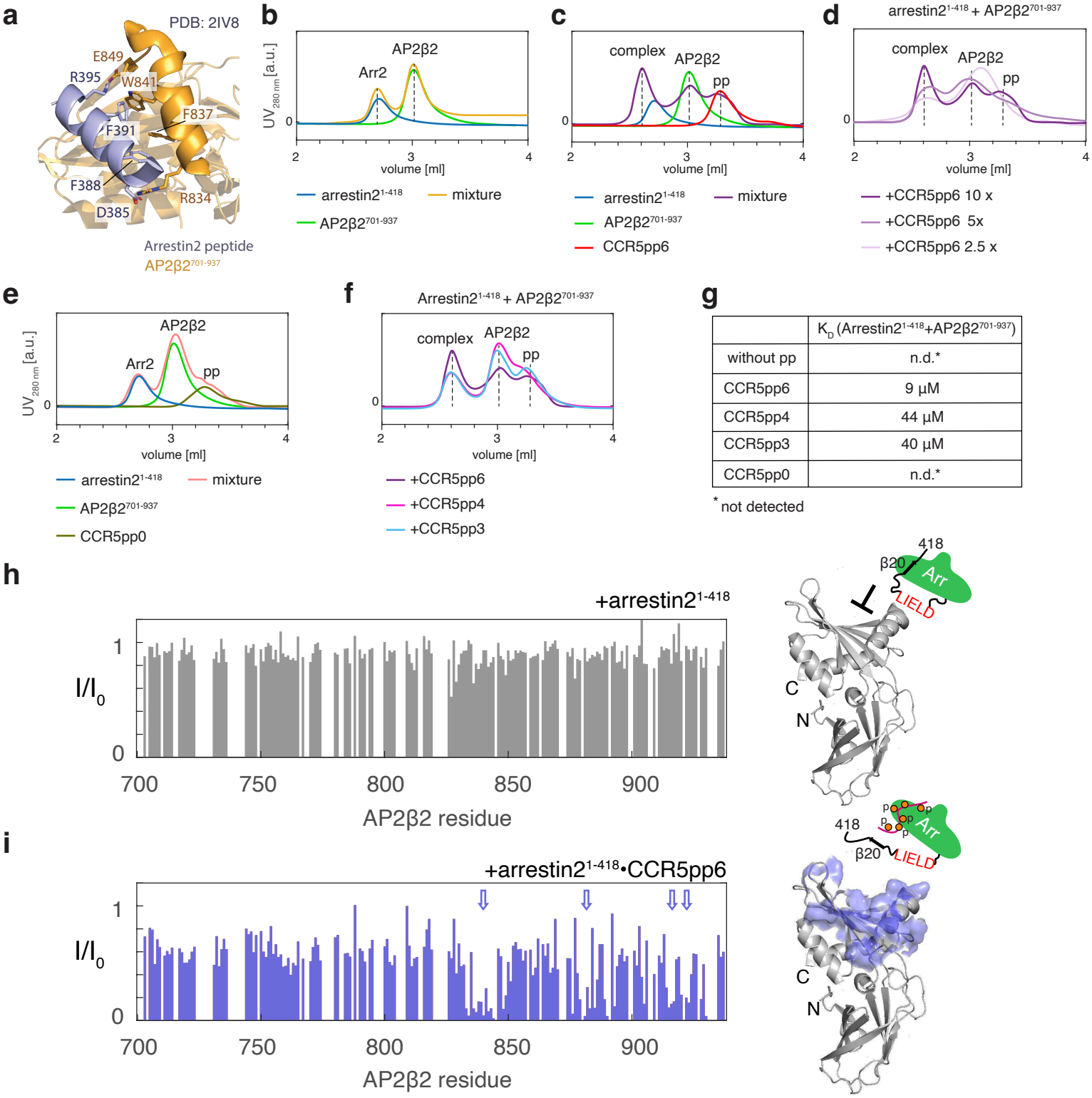

	K_D (Arrestin2$^{1-418}$+AP2β2$^{701-937}$)
without pp	n.d.*
CCR5pp6	9 µM
CCR5pp4	44 µM
CCR5pp3	40 µM
CCR5pp0	n.d.*

* not detected

Figure 4

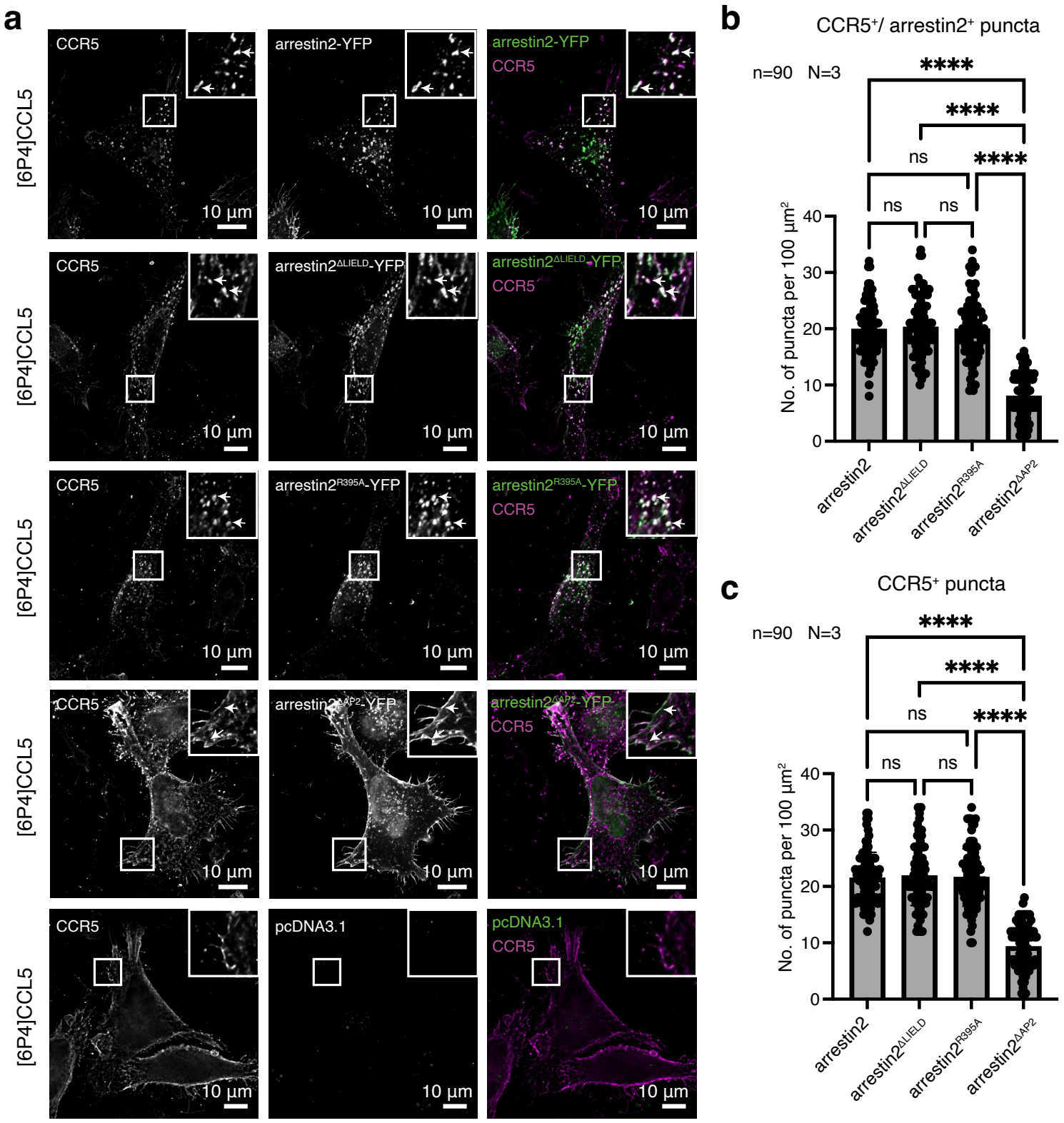
a
[6P4]CCL5
CCR5
arrestin2-YFP
arrestin2-YFP
CCR5
arrestin2ΔLIELD-YFP
arrestin2ΔLIELD-YFP
arrestin2R395A-YFP
arrestin2R395A-YFP
arrestin2ΔAP2-YFP
arrestin2ΔAP2-YFP
pcDNA3.1
pcDNA3.1
10 µm
b
CCR5+/ arrestin2+ puncta
n=90 N=3
****
****
ns
****
ns
ns
No. of puncta per 100 µm2
0
10
20
30
40
arrestin2
arrestin2ΔLIELD
arrestin2R395A
arrestin2ΔAP2
c
CCR5+ puncta
n=90 N=3
****
****
ns
****
ns
ns
No. of puncta per 100 µm2
0
10
20
30
40
arrestin2
arrestin2ΔLIELD
arrestin2R395A
arrestin2ΔAP2

Figure 5

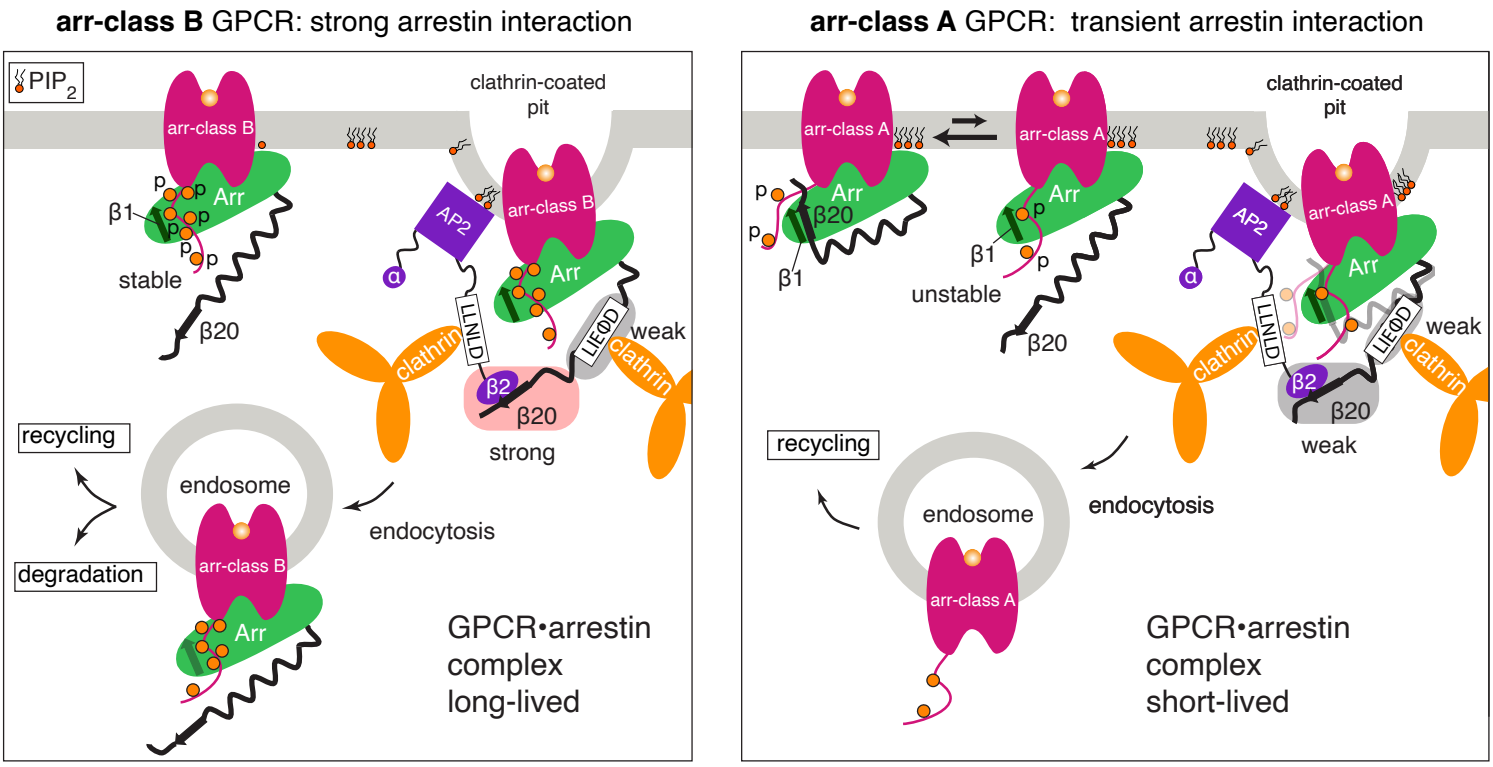
arr-class B GPCR: strong arrestin interaction
PIP2
clathrin-coated pit
arr-class B
Arr
β1
p
stable
β20
AP2
α
LLNLD
β2
strong
LIEΦD
weak
clathrin
recycling
endosome
endocytosis
degradation
GPCR•arrestin complex long-lived
arr-class A GPCR: transient arrestin interaction
arr-class A
unstable
weak
GPCR•arrestin complex short-lived

Figure 6